A Realistic Intersecting D6-Brane Model after the First LHC Run

Tianjun Li[a,b,1], D.V. Nanopoulos[c,d2], Shabbar Raza[a,3], Xiao-Chuan Wang[a,4]

[a] *State Key Laboratory of Theoretical Physics and Kavli Institute for Theoretical Physics China (KITPC), Institute of Theoretical Physics, Chinese Academy of Sciences, Beijing 100190, P. R. China*

[b] *School of Physical Electronics, University of Electronic Science and Technology of China, Chengdu 610054, P. R. China*

[c] *George P. and Cynthia W. Mitchell Institute for Fundamental Physics, Texas A&M University, College Station, Texas 77843, USA*

[d] *Astroparticle Physics Group, Houston Advanced Research Center (HARC), Mitchell Campus, Woodlands, Texas 77381, USA and Academy of Athens, Division of Natural Sciences, 28 Panepistimiou Avenue, Athens 10679, Greece*

Abstract

With the Higgs boson mass around 125 GeV and the LHC supersymmetry search constraints, we revisit a three-family Pati-Salam model from intersecting D6-branes in Type IIA string theory on the $\mathbf{T^6}/(\mathbb{Z}_\mathbf{2} \times \mathbb{Z}_\mathbf{2})$ orientifold which has a realistic phenomenology. We systematically scan the parameter space for $\mu < 0$ and $\mu > 0$, and find that the gravitino mass is generically heavier than about 2 TeV for both cases due to the Higgs mass low bound 123 GeV. In particular, we identify a region of parameter space with the electroweak fine-tuning as small as $\Delta_{EW} \sim$ 24-32 (3-4%). In the viable parameter space which is consistent with all the current constraints, the mass ranges for gluino, the first two-generation squarks and sleptons are respectively [3, 18] TeV, [3, 16] TeV, and [2, 7] TeV. For the third-generation sfermions, the light stop satisfying 5σ WMAP bounds via neutralino-stop coannihilation has mass from 0.5 to 1.2 TeV, and the light stau can be as light as 800 GeV. We also show various coannihilation and resonance scenarios through which the observed dark matter relic density is achieved.

[1]E-mail: tli@itp.ac.cn
[2]E-mail: dimitri@physics.tamu.edu
[3]E-mail: shabbar@itp.ac.cn
[4]E-mail: xcwang@itp.ac.cn

Interestingly, the certain portions of parameter space has excellent t-b-τ and b-τ Yukawa coupling unification. Three regions of parameter space are highlighted as well where the dominant component of the lightest neutralino is a bino, wino or higgsino. We discuss various scenarios in which such solutions may avoid recent astrophysical bounds in case if they satisfy or above observed relic density bounds. Prospects of finding higgsino-like neutralino in direct and indirect searches are also studied. And we display six tables of benchmark points depicting various interesting features of our model. Note that the lightest neutralino can be heavy up to 2.8 TeV, and there exists a natural region of parameter space from low-energy fine-tuning definition with heavy gluino and first two-generation squarks/sleptons, we point out that the 33 TeV and 100 TeV proton-proton colliders are indeed needed to probe our D-brane model.

1 Introduction

String theory is one of the most promising candidates for quantum gravity. Thus, the string phenomenology goal is to construct the Standard Model (SM) or Supersymmetric SMs (SSMs) from string theory with moduli stabilization and without chiral exotics, and try to make unique predictions which can probed at the Large Hadron Collider (LHC) and other future experiments. It is well-known that four kinds of string models have been studied extensively: (1) The heterotic $E_8 \times E_8$ string model building. The SSMs can be constructed via the orbifold compactifications [1, 2, 3] and the Calabi-Yau manifold compactifications [4, 5]. (2) The free fermionic string model building. The realistic models with clean particle spectra such as the standard-like models, Pati-Salam models, and flipped $SU(5)$ models have been constructed at the Kac-Moody level one [6, 7, 8, 9, 10]. (3) The D-brane model building. Two kinds of such models have been studied: (i) Intersecting D-brane models [11, 12, 13, 14, 15, 16, 17, 18, 19, 20, 21]; (ii) Orientifolds of Gepner models [22, 23]. (4) The F-theory model building for the $SU(5)$, flipped $SU(5)$, and $SU(3)_C \times SU(2)_L \times SU(2)_R \times U(1)_{B-L}$ models [24, 25, 26, 27, 28, 29, 30, 31, 32].

For the intersecting D-brane model building, the realistic SM fermion Yukawa couplings can be realized only in the Pati-Salam models. The three-family Pati-Salam models have been constructed systematically in Type IIA string theory on the $\mathbf{T^6}/(\mathbb{Z}_\mathbf{2} \times \mathbb{Z}_\mathbf{2})$ orientifold with intersecting D6-branes [16], and two of us (TL and DVN) with Chen and Mayes found that one model has a realistic phenomenology: the tree-level gauge coupling unification is realized naturally at the string scale, the Pati-Salam gauge symmetry can be broken to the SM close to the string scale, the small number of extra chiral exotic states may be decoupled via the Higgs mechanism and strong dynamics, the SM fermion masses and mixings can be explained, the low-energy supersymmetric particle spectra might potentially be tested at the LHC, and the observed dark matter relic density may be generated for the lightest neutralino as the lightest supersymmetric particle (LSP), etc [33, 34]. As far as we know, this is indeed one of the best globally consistent string models.

On the other hand, for the first run of the LHC, the big success is obviously the discovery of a SM-like Higgs boson with mass m_h around 125 GeV in July 2012 [35, 36], which is a little bit too large for the Minimal SSM (MSSM). Such large Higgs boson mass in the MSSM requires the multi-TeV top squarks with small mixing or TeV-scale top squarks with large mixing. In addition, the LHC supersymmetry (SUSY) searches have given strong constraints on the pre-LHC viable parameter space. For instance, the gluino mass $m_{\tilde{g}}$ should be heavier than about 1.7 TeV if the first two-generation squark mass $m_{\tilde{q}}$ is around the gluino mass $m_{\tilde{q}} \sim m_{\tilde{g}}$, and heavier than about 1.3 TeV for $m_{\tilde{q}} \gg m_{\tilde{g}}$ [37, 38].

Therefore, we should update the phenomenological study of this intersecting D-brane model.

For this purpose, we have systematically scan the viable parameter space by considering $\mu < 0$ and $\mu > 0$ scenarios where μ is the bilinear Higgs mass term. We show that there indeed exists such viable parameter space which satisfies the collider and astrophysical bounds including the Higgs boson mass in the range $[123, 127]$ GeV. In particular, the absolute value of μ can be as small as 300 GeV in a region of parameter space, where the electroweak fine-tuning (EWFT) is small around $\Delta_{EW} \sim$ 24-32 (3-4%). We identify another region of parameter space with $|\mu| \lesssim$ 500 GeV and $\Delta_{EW} \lesssim 300$, where gluino masses are from 3 to 7 TeV, and the first two-generation squarks and sleptons are in the mass ranges of $[4,\ 7]$ TeV and $[2,\ 4]$ TeV, respectively. Because such parameter space is natural from the low-energy fine-tuning definition while the gluino and first two-generation squarks/sleptons are out of the reach of 14 TeV LHC, this will provide a strong motivation for the 33 TeV and 100 TeV proton-proton colliders. There is some visible preference to achieve the viable parameter space consistent with constraints for $\mu < 0$ case, but this is just an artifact of lack of statistics for $\mu > 0$. Moreover, in order to have the Higgs boson mass from 123 GeV to 127 GeV, and satisfy the LHC low bounds on sparticles and the B-physics bounds, we require gravitino mass $\gtrsim$ 2 TeV for both cases of $\mu < 0$ and $\mu > 0$. We also present graphs in neutralino-sparticle planes showing various coannihilation scenarios such as neutralino-stau, neutralino-stop, neutralino-gluino, and A-resonance solutions. The solutions, which are consistent with the observed relic density, have gluino masses from 3 to 18 TeV. We also note that in our present data consistent with all bounds, the first two generation squarks are in the mass range $[3,\ 16]$ TeV and the first two generation sleptons can be heavier than 2 TeV but less than 6 TeV. On the other hand for third family squarks, the NLSP light stop satisfying 5σ WMAP bounds is in the mass of 0.5-1.2 TeV, in case of third family slepton, the light stau can be as light as 800 GeV. We have checked status of t-b-τ and b-τ Yukawa unification (YU) scenarios with both signs of μ in our data. For $\mu < 0$ we find solutions with 10% or better YU with typical heavy spectra. The best YU we have achieved in our data set is about 5% consistent with all the constraints including the observed dark matter relic density bound. On the other hand, we do not have better than 12% YU t-b-τ for $\mu > 0$ case. Since we did not perform any dedicate searches to study YU in this project otherwise we may have solutions with much better YU. Relaxing the t-b-τ YU constraint to b-τ YU, we have plenty of solutions with 100% YU. For the points with $\Omega h^2 \gtrsim 1$ where the lightest neutralino is almost a pure bino, we introduce a lighter state axino $\tilde{a}$ as the LSP. Thus, the lightest neutralino is the Next to the LSP (NLSP) and can decay to axino via $\tilde{\chi}_1^0 \to \gamma\tilde{a}$. We calculate the lifetime of the NLSP neutralino for various choices of the axion decay constant f_a in our data. For $f_a > 10^{14}$ GeV, the lifetime of the NLSP bino is more than 1 second and may be ruled out by Big Bang Nucleosynthesis (BBN) constraints. We also note that in

our data, there are solutions where the lightest neutralino can be a bino, wino, or higgsino type. The lightest neutralino masses are more than 1 TeV for both cases ($\mu < 0$ and $\mu > 0$) in the wino-type solutions, while they are less than 1 TeV in the bino-type solutions and in the mass range of 150-600 GeV in the higgsino-type solutions. Recent studies showed that the scenario with pure wino as dark matter is under siege [39, 40]. In our model, the relic density of the wino dominant lightest neutralino can be smaller than the correct relic density, and then the above constraint can be escaped. Otherwise, to solve this problem, we suggest that the wino dominant neutralino is the NLSP and may decay to $\tilde{a}\gamma$ and hence fulfil the relic density bounds, or we may invoke R-parity violation. Similarly, the higgsino-type solutions suffer underabundance of relic density problem. In such a case we assume that the higgsino-type neutralino makes up only a fraction of the dark matter relic density and the remaining abundance is comprised of axions. We also display graphs for direct and indirect searches for dark matter for our higgsino-like solutions and show that these solutions will be observed or ruled out by the XENON1T experiment. Finally, we present six tables of benchmark points, three for each sign of μ. These points depict various interesting scenarios of our model, namely points with minimum EWFT, various coannihilation and resonance solutions, bino-type, wino-type and higgsino-type solutions. Furthermore, because the lightest neutralino can be heavier than 1 TeV and up to about 2.8 TeV, how to search for such scenario at the 14 TeV LHC is still a challenging question. In short, we do need the 33 TeV and 100 TeV proton-proton colliders to probe such D-brane model.

This paper is organized as follows. In Section 2 we outline details of the supersymmetry breaking (SSB) parameters, the range of values employed in our scan, the scanning procedure and the relevant experimental constraints that we have employed. In Section 3 we briefly describe our definition of EWFT and High scale (GUT) fine-tuning. We discuss results of our scans in Section 4. A summary and conclusions are given in Section 5.

2 Phenomenological constraints and scanning procedure

In our realistic intersecting D-brane model, if we do not consider CP violation, the supersymmetry breaking (SSB) soft terms from the non-zero F-terms F^{u^i} and F^s can be parametrized by Θ_1, Θ_2, Θ_3, $\Theta_4 \equiv \Theta_s$, and gravitino mass $m_{3/2}$ where $\sum_{i=1}^{4} \Theta_i^2 = 1$ [34]. Thus, we can

reparametrize Θ_i with $i = 1,\ 2,\ 3$ in terms of γ_1, γ_2 and Θ_4 as follows

$$\begin{aligned}
\alpha &\equiv 2\pi\gamma_1 \ , \\
\beta &\equiv 2\pi\gamma_2 \ , \\
\Theta_1 &= \cos(\beta)\cos(\alpha)\sqrt{1-\Theta_4^2} \ , \\
\Theta_2 &= \cos(\beta)\sin(\alpha)\sqrt{1-\Theta_4^2} \ , \\
\Theta_3 &= \sin(\beta)\sqrt{1-\Theta_4^2} \ . \qquad (1)
\end{aligned}$$

Thus, the supersymmetry breaking soft terms are [34]

$$\begin{aligned}
M_1 &= (0.519\Theta_1 + 0.346\Theta_2 + 0.866\Theta_3)m_{3/2} \ , \\
M_2 &= (0.866\Theta_2 - 0.866\Theta_4)m_{3/2} \ , \\
M_3 &= (0.866\Theta_2 + 0.866\Theta_3)m_{3/2} \ , \\
A_0 &= (-1.111\Theta_1 - 0.621\Theta_2 + 0.245\Theta_3 - 0.245\Theta_4)m_{3/2} \ , \\
m_L &= \sqrt{(1.0 + 0.899\Theta_1^2 - 0.518\Theta_2^2 - 0.849\Theta_3^2 - 1.418\Theta_4^2 - 0.557\Theta_1\Theta_2 - 0.557\Theta_3\Theta_4)}m_{3/2} \ , \\
m_R &= \sqrt{(1.0 - 1.418\Theta_1^2 - 0.849\Theta_2^2 - 0.518\Theta_3^2 + 0.899\Theta_4^2 - 0.557\Theta_1\Theta_2 - 0.557\Theta_3\Theta_4)}m_{3/2} \ , \\
m_{H_u} &= m_{H_d} = \sqrt{(1.0 - (1.5\Theta_3^2) - (1.5\Theta_4^2))}m_{3/2} \ , \qquad (2)
\end{aligned}$$

where $M_{1,2,3}$ are the gauginos masses respectively for $U(1)_Y$, $SU(2)_L$ and $SU(3)_c$ gauge groups, A_0 is the trilinear scalar coupling, m_L and m_R are the soft mass terms respectively for the left-handed and right-handed squarks and sleptons, and $m_{H_{u,d}}$ are the SSB Higgs soft mass terms.

We employ the ISAJET 7.84 package [41] to perform random scans over the parameter space given below. In this package, the weak scale values of gauge and third generation Yukawa couplings are evolved to $M_{\rm GUT}$ via the MSSM renormalization group equations (RGEs) in the $\overline{DR}$ regularization scheme. We do not strictly enforce the unification condition $g_3 = g_1 = g_2$ at $M_{\rm GUT}$, since a few percent deviation from unification can be assigned to unknown GUT-scale threshold corrections [42]. With the boundary conditions given at $M_{\rm GUT}$, all the SSB parameters, along with the gauge and Yukawa couplings, are evolved back to the weak scale $M_{\rm Z}$.

In evaluating Yukawa couplings the SUSY threshold corrections [43] are taken into account at the common scale $M_{\rm SUSY} = \sqrt{m_{\tilde{t}_L} m_{\tilde{t}_R}}$. The entire parameter set is iteratively run between $M_{\rm Z}$ and $M_{\rm GUT}$ using the full 2-loop RGEs until a stable solution is obtained. To better account for leading-log corrections, one-loop step-beta functions are adopted for gauge and Yukawa couplings, and the SSB parameters m_i are extracted from RGEs at appropriate scales $m_i = m_i(m_i)$.

The RGE-improved 1-loop effective potential is minimized at an optimized scale $M_{\rm SUSY}$, which effectively accounts for the leading 2-loop corrections. Full 1-loop radiative corrections are incorporated for all sparticle masses.

The requirement of radiative electroweak symmetry breaking (REWSB) [44] puts an important theoretical constraint on the parameter space. Another important constraint comes from limits on the cosmological abundance of stable charged particle [45]. This excludes regions in the parameter space where charged SUSY particles, such as $\tilde{\tau}_1$ or $\tilde{t}_1$, become the LSP. We accept only those solutions for which one of the neutralinos is the LSP and saturates the dark matter relic abundance bound observed by WMAP9.

We have performed Markov-chain Monte Carlo (MCMC) scans for the following parameter range

$$\begin{aligned} 0 \leq & \gamma_1 \leq 1 \ , \\ 0 \leq & \gamma_2 \leq 1 \ , \\ 0 \leq & \Theta_4 \leq 1 \ , \\ 1 \leq & m_{3/2} \leq 10\,\text{TeV} \ , \\ 2 \leq & \tan\beta \leq 60 \ , \end{aligned} \tag{3}$$

where $\tan\beta$ is the ratio of the vacuum expectation values (VEVs) of two Higgs fields. We use $m_t = 173.3\,\text{GeV}$ [46], and $m_b^{\overline{DR}}(M_Z) = 2.83$ GeV which is hard-coded into ISAJET. We have done our scans with both $\mu < 0$ and $\mu > 0$, and find that our results are not too sensitive to one or two sigma variation in the value of m_t [47].

In scanning the parameter space, we employ the Metropolis-Hastings algorithm as described in [48]. The collected data points all satisfy the requirement of REWSB, with the neutralino in each case being the LSP. After collecting the data, we require the following bounds (inspired by the LEP2 experiment) on particle masses:

$$m_{\tilde{t}_1}, m_{\tilde{b}_1} \gtrsim 100 \text{ GeV} \ , \tag{4}$$

$$m_{\tilde{\tau}_1} \gtrsim 105 \text{ GeV} \ , \tag{5}$$

$$m_{\tilde{\chi}_1^\pm} \gtrsim 103 \text{ GeV} \ . \tag{6}$$

We also use IsaTools package [49, 50] and Ref. [51] to implement the following B-physics constraints:

$$0.8 \times 10^{-9} \leq \text{BR}(B_s \to \mu^+\mu^-) \leq 6.2 \times 10^{-9} \ (2\sigma) \qquad [52] \ , \tag{7}$$

$$2.99 \times 10^{-4} \leq \text{BR}(b \to s\gamma) \leq 3.87 \times 10^{-4} \ (2\sigma) \qquad [53] \ , \tag{8}$$

$$0.15 \leq \frac{\text{BR}(B_u \to \tau\nu_\tau)_{\rm MSSM}}{\text{BR}(B_u \to \tau\nu_\tau)_{\rm SM}} \leq 2.41 \ (3\sigma) \qquad [54] \ . \tag{9}$$

In addition to above constraints, we impose the following bounds from the LHC and WMAP9

$$m_h = 123 - 127 \text{ GeV} \quad [55,\ 56] \ , \tag{10}$$

$$m_{\tilde{g}} \gtrsim 1.7 \,\text{TeV} \ (\text{for } m_{\tilde{g}} \sim m_{\tilde{q}}) \quad [37,\ 38] \ , \tag{11}$$

$$m_{\tilde{g}} \gtrsim 1.3 \,\text{TeV} \ (\text{for } m_{\tilde{g}} \ll m_{\tilde{q}}) \quad [37,\ 38] \ , \tag{12}$$

$$0.0913 \leq \Omega_{\rm CDM} h^2(\text{WMAP9}) \leq 0.1363 \ (5\sigma) \qquad [57] \ . \tag{13}$$

As far as the muon anomalous magnetic moment a_μ is concerned, we require that the benchmark points are at least as consistent with the data as the Standard Model.

3 Fine-Tuning

We use the latest (7.84) version of ISAJET [41] to calculate the fine-tuning (FT) conditions at the electroweak scale (EW) M_{EW} and at the high scale (M_{HS}). Brief description of these parameters is given in this section.

The Z boson mass M_Z, after including the one-loop effective potential contributions to the tree level MSSM Higgs potential, is given by the following relation:

$$\frac{M_Z^2}{2} = \frac{(m_{H_d}^2 + \Sigma_d^d) - (m_{H_u}^2 + \Sigma_u^u)\tan^2\beta}{\tan^2\beta - 1} - \mu^2 \ , \tag{14}$$

where Σ_u^u and Σ_d^d are the contributions coming from the one-loop effective potential defined in [58]) and $\tan\beta \equiv \langle H_u\rangle/\langle H_d\rangle$. All parameters in Eq. (14) are defined at the M_{EW}.

3.1 Electroweak Scale Fine-Tuning

We follow [58] in order to measure the EW scale fine-tuning condition, the following definitions are used:

$$C_{H_d} \equiv |m_{H_d}^2/(\tan^2\beta - 1)|, \ C_{H_u} \equiv |-m_{H_u}^2 \tan^2\beta/(\tan^2\beta - 1)|, \ C_\mu \equiv |-\mu^2|, \tag{15}$$

with each $C_{\Sigma_{u,d}^{u,d}(k)}$ less than some characteristic value of order M_Z^2. Here, k labels the SM and SUSY particles that contribute to the one-loop Higgs potential. For the fine-tuning condition we have

$$\Delta_{\rm EW} \equiv \max(C_k)/(M_Z^2/2) \ . \tag{16}$$

It is important to note that Δ_{EW} depends only on the weak scale parameters of the theory, therefore fixed by the particle spectrum. Hence, it is independent of how SUSY particle masses arise. Lower values of Δ_{EW} correspond to less fine tuning, for example, $\Delta_{EW} = 10$ implies $\Delta_{EW}^{-1} = 10\%$ fine tuning. Moreover, this condition of EW scale fine-tuning is different from the fine-tuning definition in Refs. [59, 60] beyond the tree level (for more details see [61]).

3.2 High Scale Fine-Tuning

From Eq. (14) it is evident that Δ_{EW} does not give any informations about the possible high scale origin of the parameters in the equation. In order to address fully the fine-tuning condition we need to write down weak-scale parameter $m^2_{H_{u,d}}$ in Eq. (14) and with their explicit dependence on the (HS) as:

$$m^2_{H_{u,d}} = m^2_{H_{u,d}}(M_{HS}) + \delta m^2_{H_{u,d}}, \quad \mu^2 = \mu^2(M_{HS}) + \delta\mu^2. \tag{17}$$

Here $m^2_{H_{u,d}}(M_{HS})$ and $\mu^2(M_{HS})$ are the corresponding parameters renormalized at the high scale, and $\delta m^2_{H_{u,d}}$, and $\delta\mu^2$ measure how the given parameter is changed due to Renormalization Group Equation (RGE) evolution. Eq. (14) can be re-expressed in the form

$$\begin{aligned} \frac{m_Z^2}{2} &= \frac{(m^2_{H_d}(M_{HS}) + \delta m^2_{H_d} + \Sigma^d_d) - (m^2_{H_u}(M_{HS}) + \delta m^2_{H_u} + \Sigma^u_u)\tan^2\beta}{\tan^2\beta - 1} \\ &- (\mu^2(M_{HS}) + \delta\mu^2)\ . \end{aligned} \tag{18}$$

As we did before, we follow Ref. [58] and introduce the following parameters

$$\begin{gathered} B_{H_d} \equiv |m^2_{H_d}(M_{HS})/(\tan^2\beta - 1)|, B_{\delta H_d} \equiv |\delta m^2_{H_d}/(\tan^2\beta - 1)|, \\ B_{H_u} \equiv |-m^2_{H_u}(M_{HS})\tan^2\beta/(\tan^2\beta - 1)|, B_\mu \equiv |\mu^2(M_{HS})|, \\ B_{\delta H_u} \equiv |-\delta m^2_{H_u}\tan^2\beta/(\tan^2\beta - 1)|, B_{\delta\mu} \equiv |\delta\mu^2|, \end{gathered} \tag{19}$$

and the high scale fine-tuning measure $\Delta_{\rm HS}$ is defined to be

$$\Delta_{\rm HS} \equiv \max(B_i)/(M_Z^2/2). \tag{20}$$

In short, Δ_{EW} includes information about the minimal amount of fine-tuning present in the low scale model for a given SUSY spectrum, while Δ_{HS} better represents the fine-tuning that is present in high scale model.

4 Numerical Results

In Fig. 1, we present graphs for various parameter given in Eq. (3). The left and the right panels show solutions for $\mu < 0$ and $\mu > 0$ scenarios, respectively. Color coding is given as, grey points satisfy REWSB and neutralino as an LSP conditions. Aqua points satisfy the mass bounds and B-physics bounds. Magenta points are subset of aqua points and also represent 123 GeV $\leqslant m_h \leqslant$ 127 GeV. Red points are subset of magenta points and also satisfy WMAP9 5σ bounds.

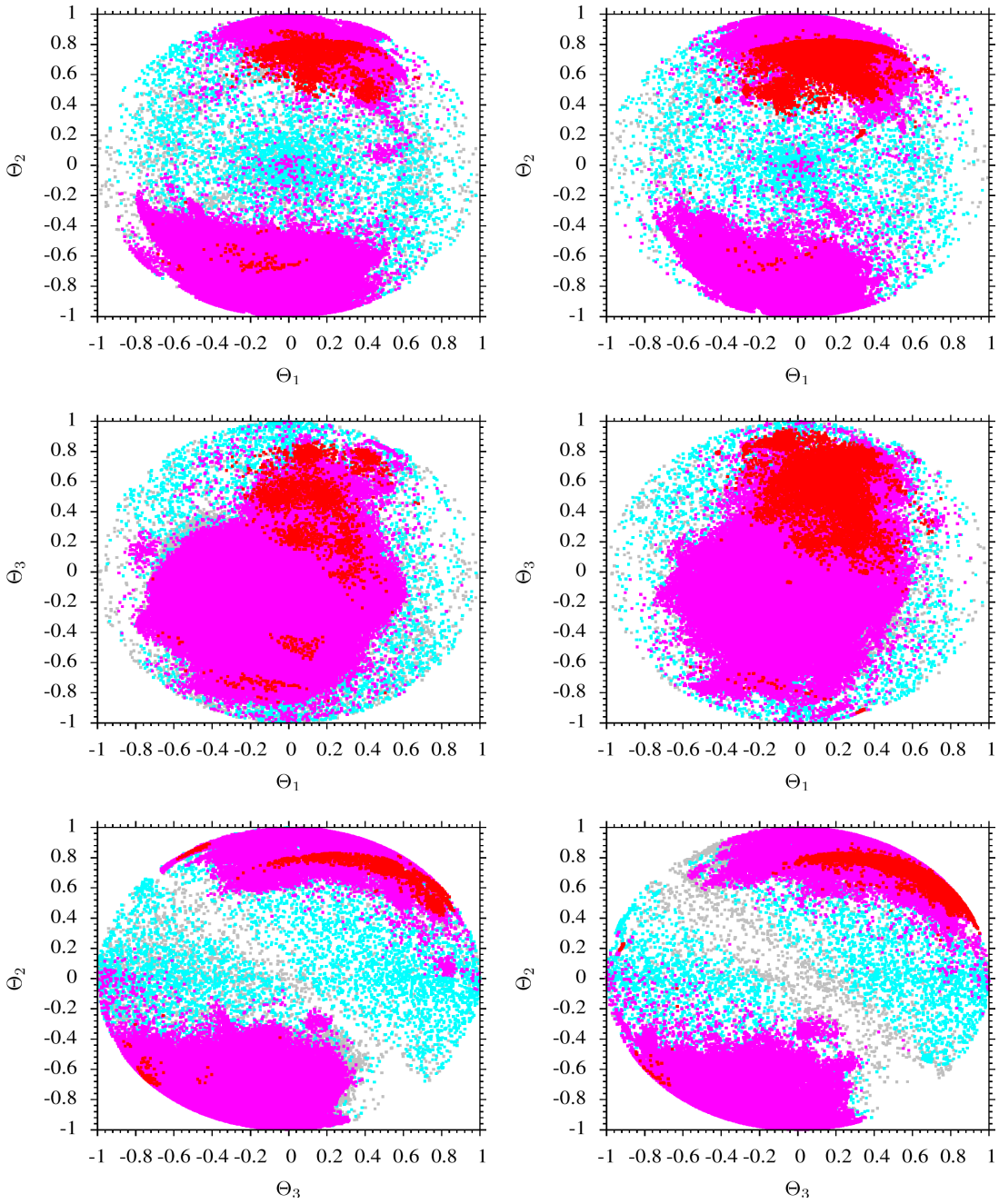

Figure 1: Plots in $\Theta_1 - \Theta_2$, $\Theta_1 - \Theta_3$ and $\Theta_3 - \Theta_2$ planes for $\mu < 0$ (left panels) and $\mu > 0$ (right panels). Grey points satisfy the REWSB and yield LSP neutralino. Aqua points satisfy all the mass bounds and B-physics bounds. Magenta points are subset of aqua points and also represent 123 GeV $\leqslant m_h \leqslant$ 127 GeV. Red points are subset of magenta points and also satisfy WMAP9 5σ bounds.

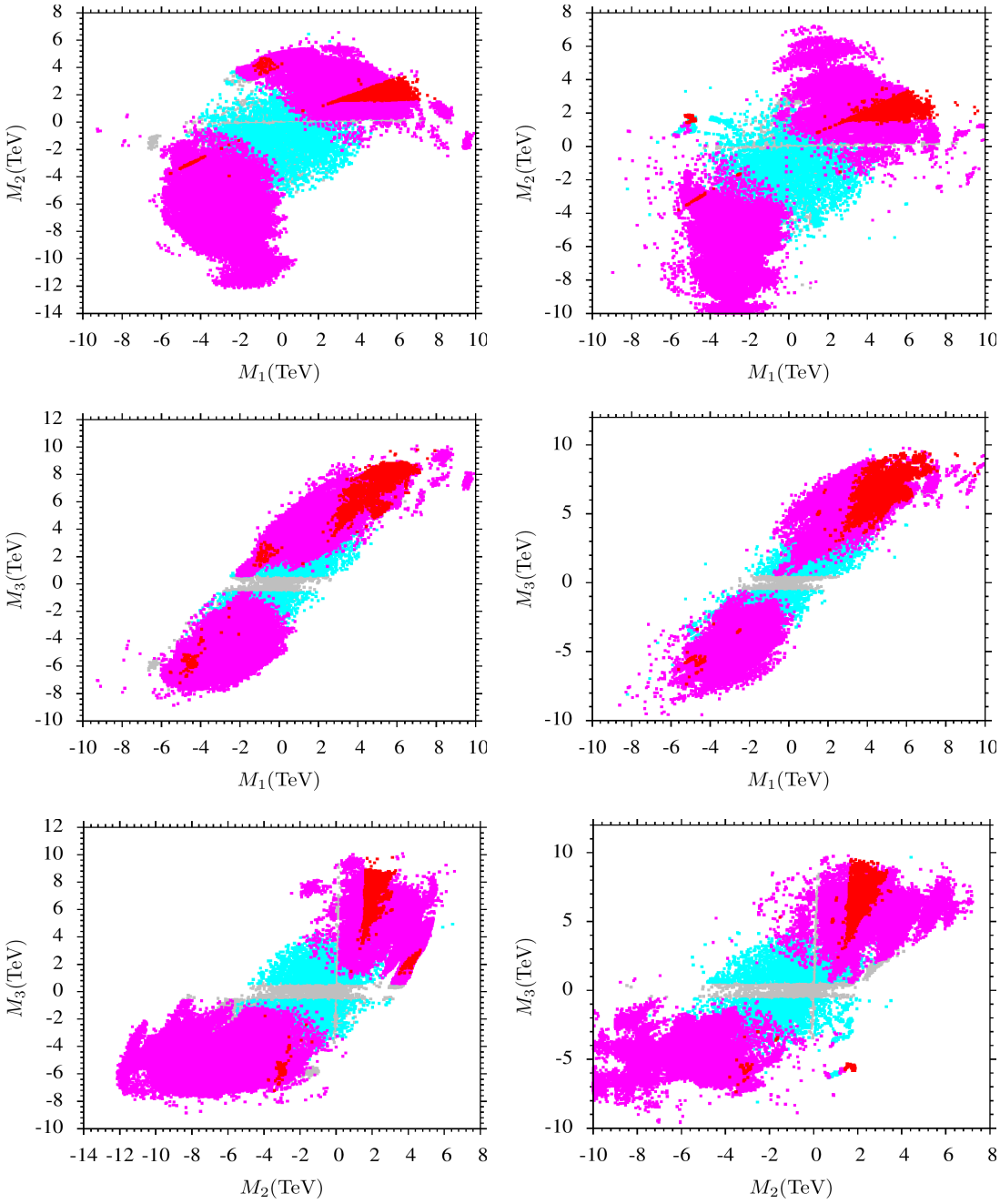

Figure 2: Plots in $M_1 - M_2$, $M_1 - M_3$ and $M_3 - M_2$ planes. Color coding and panel description are same as in Fig. 1.

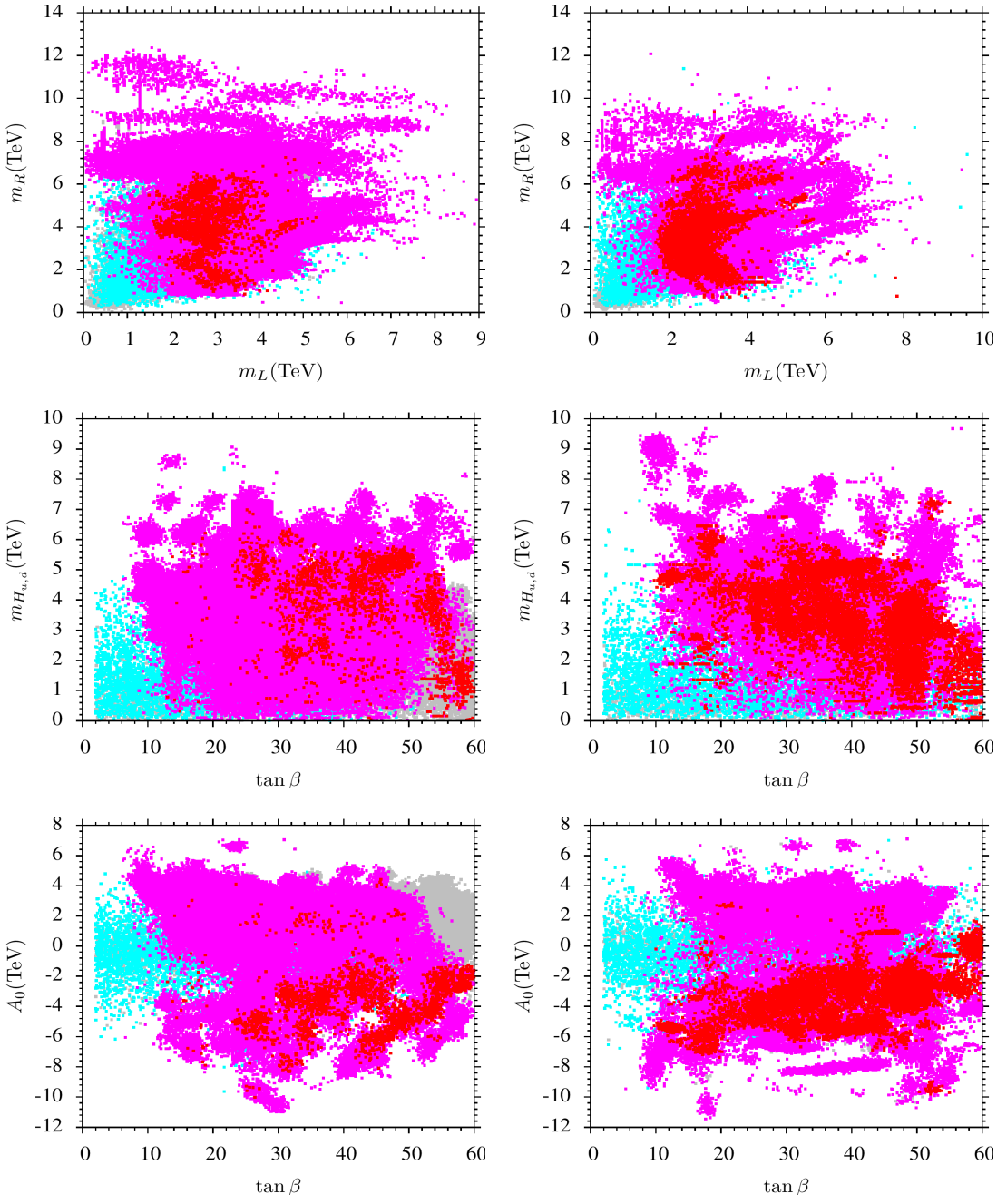

Figure 3: Plots in $m_L - m_R$, $\tan\beta - m_{H_{u,d}}$ and $\tan\beta - A_0$ planes. Color coding and panel description are same as in Fig. 1.

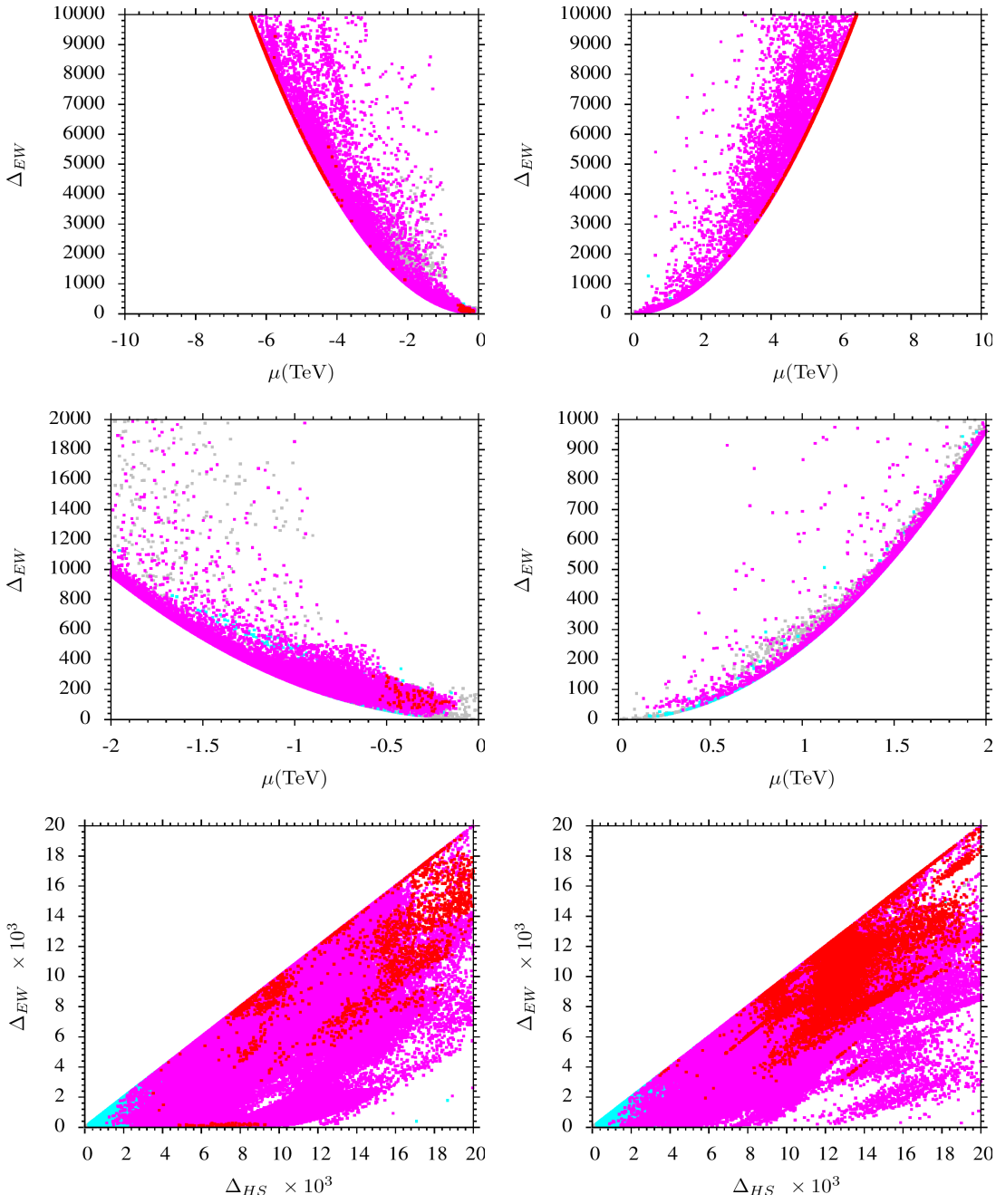

Figure 4: Plots in $\mu - \Delta_{EW}$ and $\Delta_{HS} - \Delta_{EW}$ planes. Color coding and panel description are same as in Fig. 1.

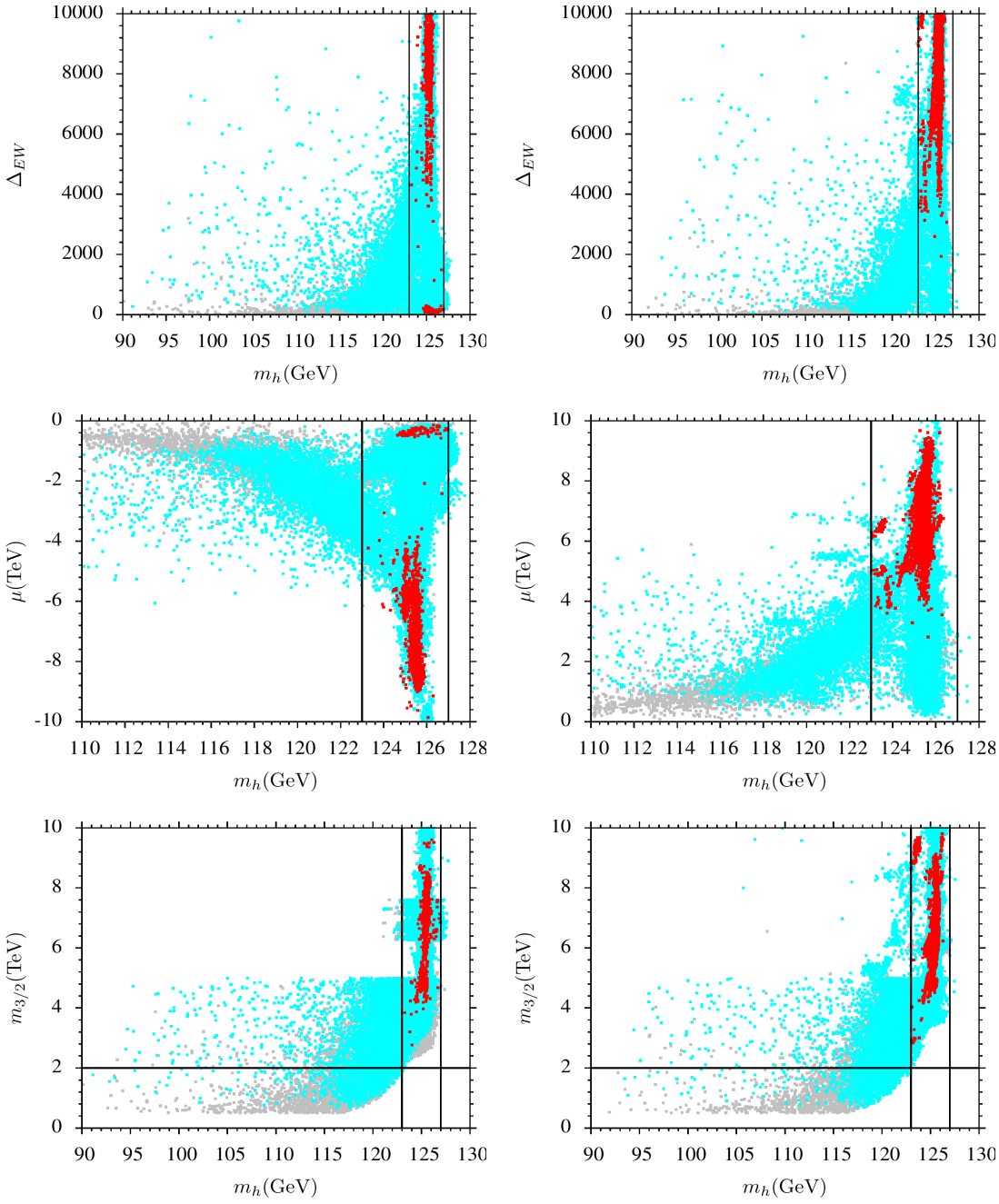

Figure 5: Plots in $m_h - \Delta_{EW}$, $m_h - \mu$ and $m_h - m_{3/2}$ planes. Grey points satisfy REWSB and yield LSP neutralino. Aqua points satisfy all the mass bounds and B-physics bounds. Red points are subset of aqua points and also satisfy the WMAP9 5σ bounds.

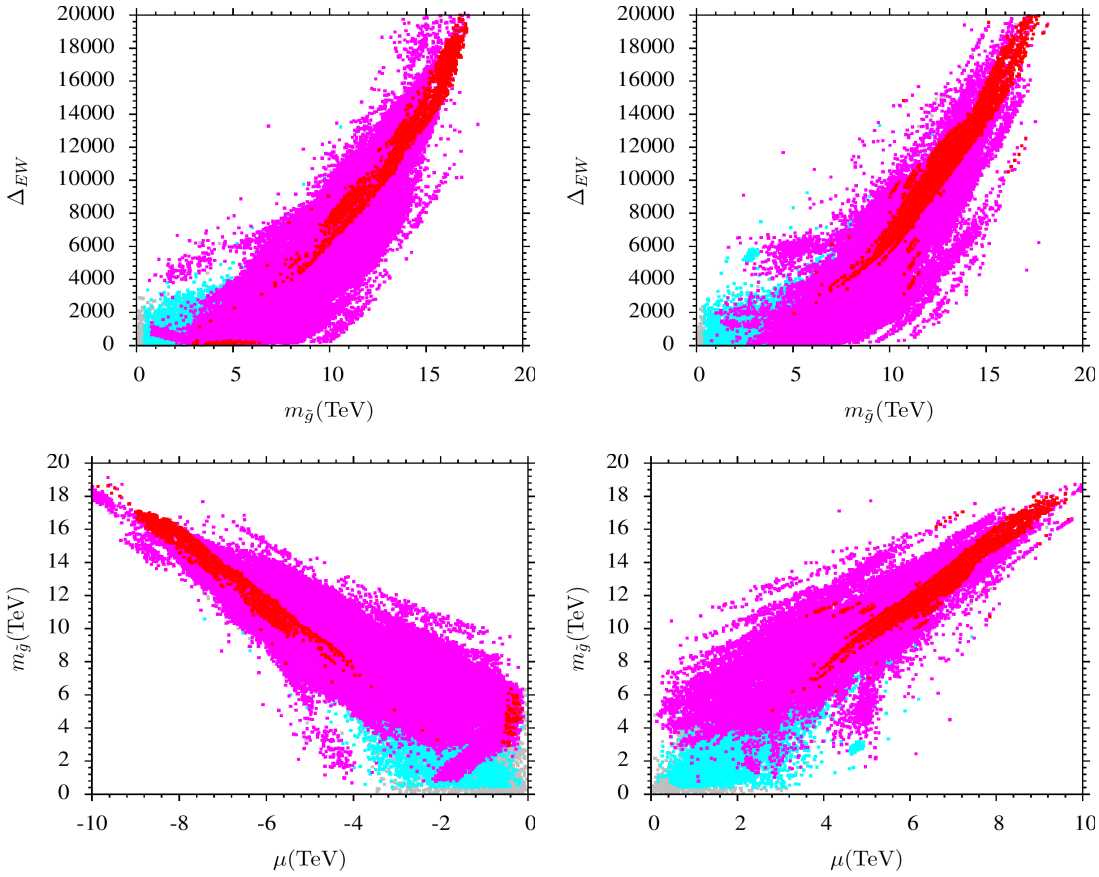

Figure 6: Plots in $\Delta_{EW} - m_{\tilde{g}}$ and $\mu - m_{\tilde{g}}$ planes. Color coding and panel description are same as in Fig. 1, except we do not apply gluino bounds mentioned in Section 2.

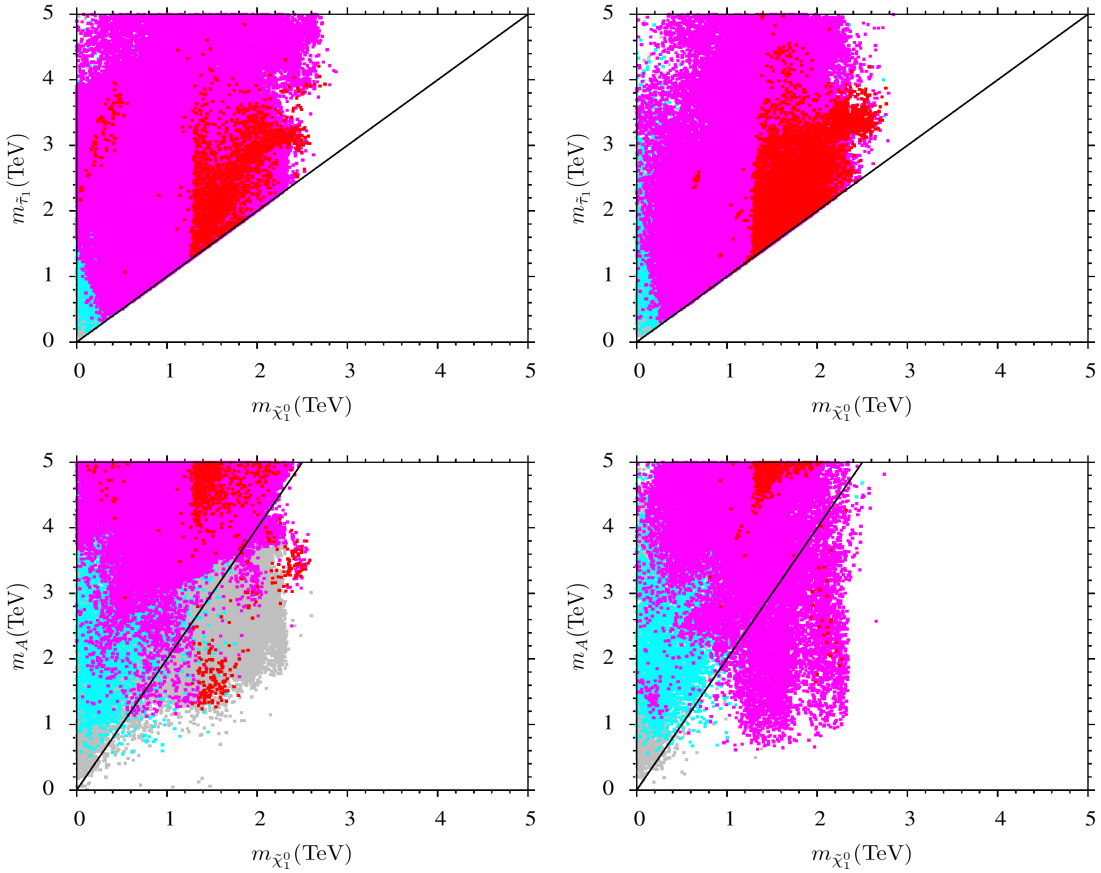

Figure 7: Plots in $m_{\tilde{\chi}_1^0} - m_{\tilde{\tau}}$ and $m_{\tilde{\chi}_1^0} - m_A$ planes. Color coding and panel description are same as in Fig. 1.

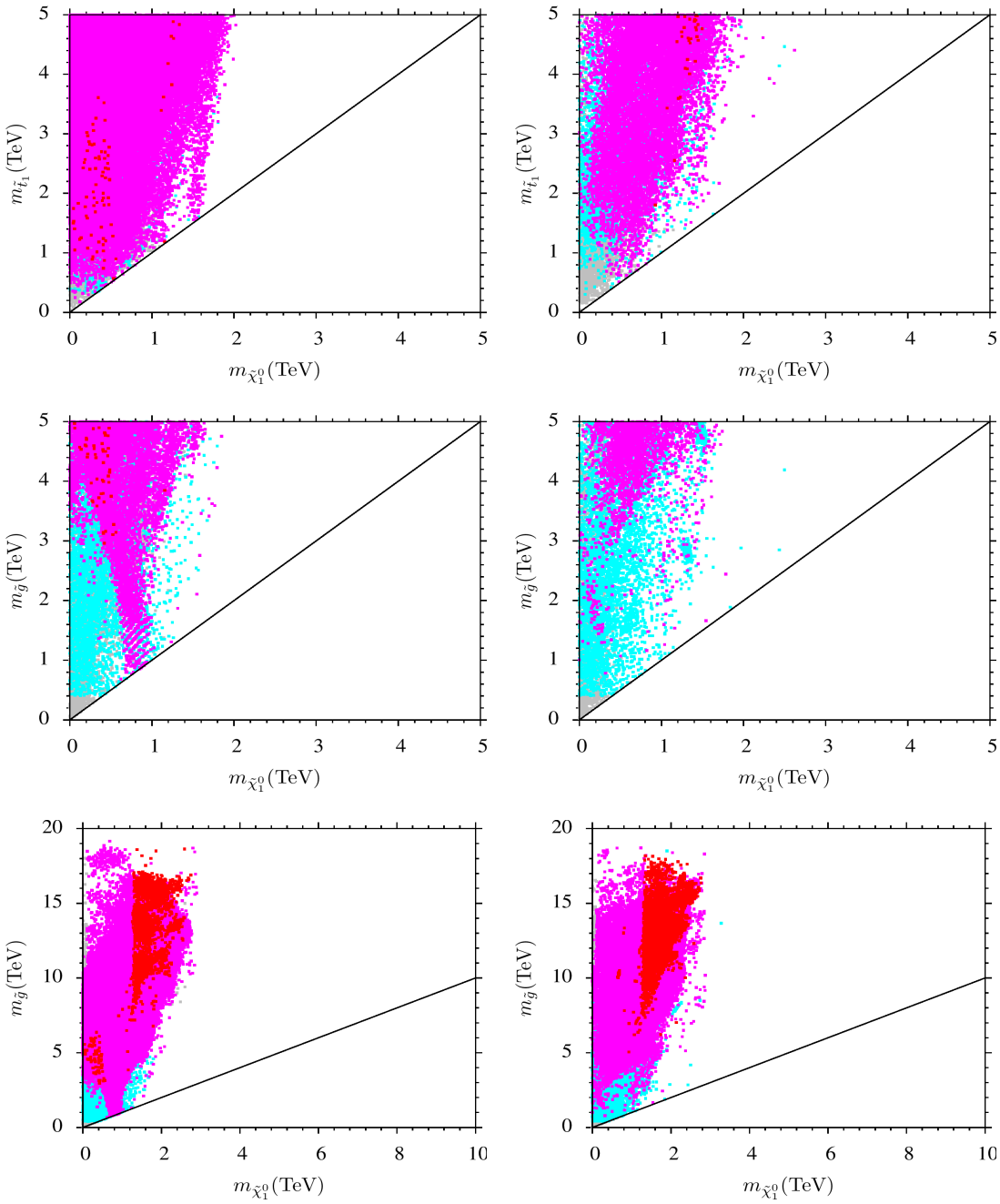

Figure 8: Plots in $m_{\tilde{\chi}_1^0} - m_{\tilde{t}_1}$ and $m_{\tilde{\chi}_1^0} - m_{\tilde{g}}$ planes. Color coding and panel description are same as in Fig. 1, except in middle and bottom panels we do not apply gluino bounds mentioned in Section 2.

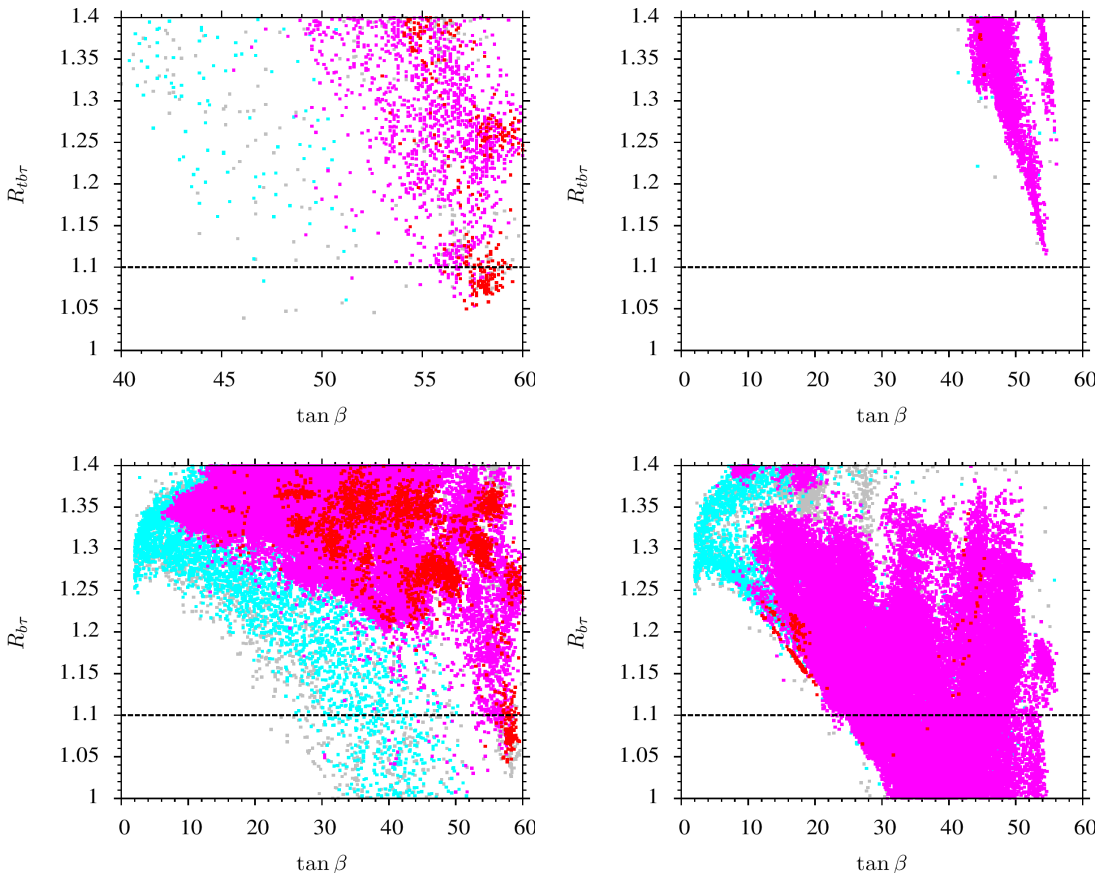

Figure 9: Plots in $\tan\beta - R_{tb\tau}$ and $\tan\beta - R_{b\tau}$ planes. Color coding and panel description are same as in Fig. 1.

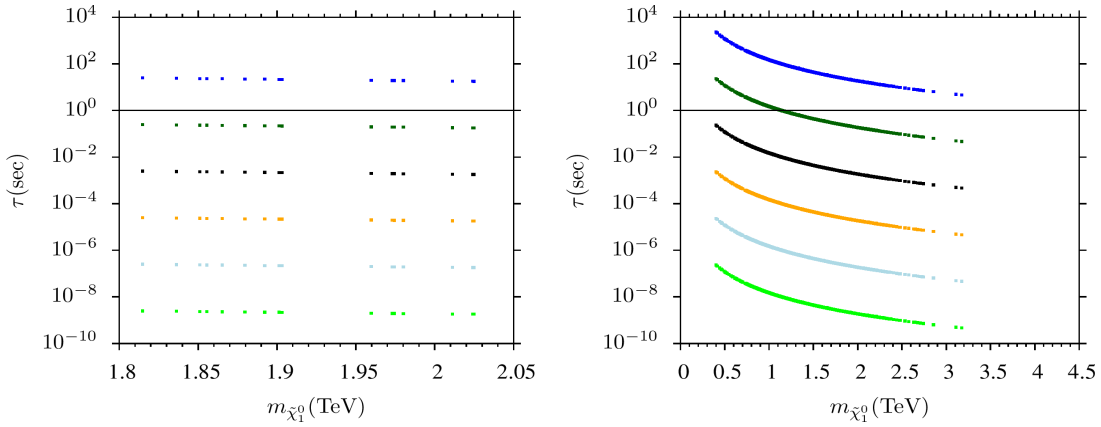

Figure 10: The NLSP bino-like neutralino mass ($m_{\tilde{\chi}_1^0}$) versus lifetime (τ) plot. We use $C_{aYY} = 8/3$, N=6. Here, light-Green, light-blue, orange, black, dark-green, and blue colors represent $f_a = 10^{10} - 10^{15}$ GeV, respectively. The black solid line shows τ =1 second.

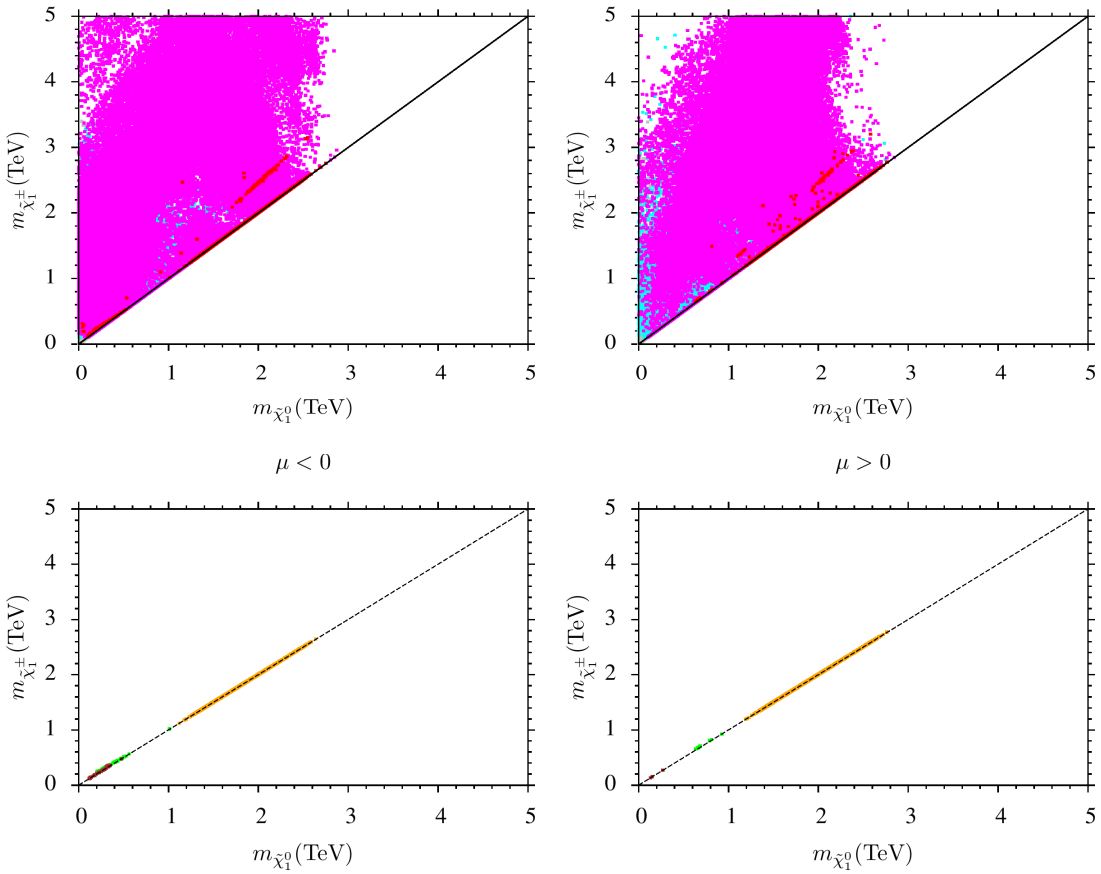

Figure 11: Plots in $m_{\tilde{\chi}_1^0} - m_{\tilde{\chi}_1^\pm}$ planes. Color coding and panel description are same as in Fig. 1 for plots in top left and right panels. In bottom left and right plots, the brown, green and orange points represent higgsino-like, bino-like, and wino-like neutralinos respectively with same panel description as in top panels.

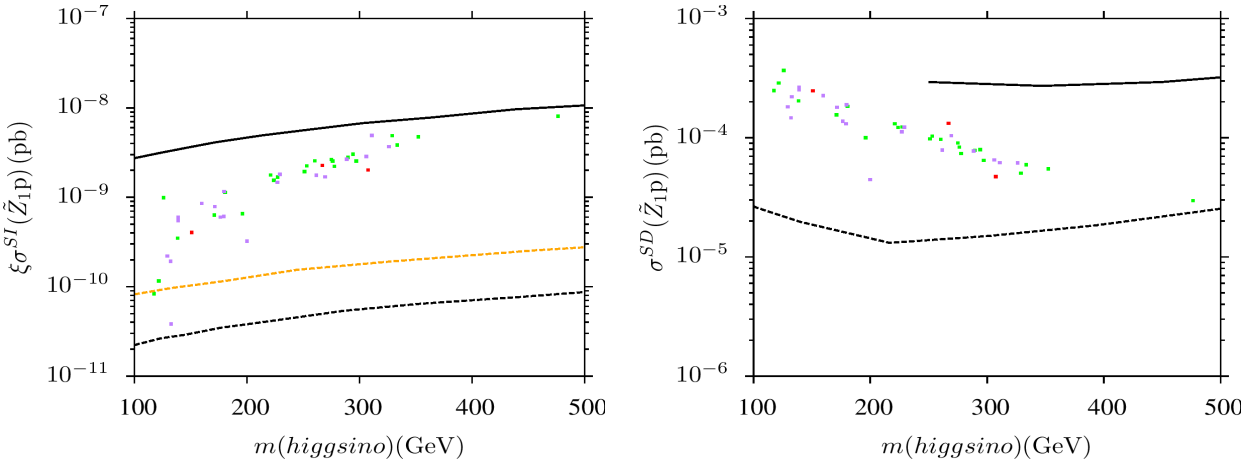

Figure 12: Plots in rescaled higgsino-like neutralino spin-independent cross section $\xi\sigma^{SI}(\tilde{Z}_1 p)$ versus m(higgsino) and (non-rescaled) higgsino-like neutralino spin-dependent cross section $\sigma^{SD}(\tilde{Z}_1 p)$ versus m(higgsino). In the left panel, the orange solid line represents the current upper bound set by the CDMS experiment and black solid line depicts the upper bound set by XENON100, while the orange and black dashed lines represent respectively the future reach of the SuperCDMS and XENON1T experiments. In the right panel, the IceCube DeepCore (black solid line) bound is shown and future IceCube DeepCore bound is depicted by the black dashed line. Green points represent solutions with $\Delta_{EW} \gtrsim$100, purple points display solutions with $50 \lesssim \Delta_{EW} \lesssim$100 while red solutions satisfy $\Delta_{EW} \lesssim$50. Here, we have combined the solutions with $\mu < 0$ and $\mu > 0$.

We see that in our scans, in $\Theta_1 - \Theta_2$ plane for both cases, the range of red points for Θ_1 is $-0.6 \lesssim \Theta_1 \lesssim 0.6$, but most of the points are concentrated in the range -0.4 to 0.4, while for Θ_2 most of the points are in the range of large values 0.4-0.8. But we also have some red points -0.6 to -0.4. On the other hand, magenta points can be more or less anywhere in the plot. We see that for Θ_1, we have solutions for its entire range in contrast to Θ_2 where points mostly have relatively large absolute values. In $\Theta_1 - \Theta_3$ plane we see that red points favor positive values of Θ_1 and Θ_3 as we have also seen in $\Theta_1 - \Theta_2$ plane. We also see some red points for small negative values of Θ_1 and but large negative values of Θ_3. Magenta points are every where but in contrast to $\Theta_1 - \Theta_2$ plane, here large density of points are around the centre of the plot. In the last panel we have plot in $\Theta_3 - \Theta_2$ plane. Here too, we see that the red points lie mostly in large positive ranges of Θ_2 and Θ_3. In case of magenta points, as compared to other panels, here we have some kind of polarisation and we do not have magenta points in the center.

We calculate (SSB) parameters using Eqs. (3) and (2). We present our results in Fig. 2. Color coding and panel description are same as in Fig. 1. In the top left and right panels we present plots in $M_1 - M_2$ plane. We note that there are some minor differences. In left panel we see that there is a patch of red points around $M_1 \sim$ -1 TeV and $M_2 \sim 4$ TeV as compare to right panel where we have some red points around $M_1 \sim$ -5 TeV and $M_2 \sim 2$ TeV. In case of magenta points, there are points up to $M_2 \sim$ -12 TeV in the left panel as compared to right panel. Similarly, we also note minor differences in other panels of the figure. In Fig. 3, plots in $m_L - m_R$, $\tan\beta - m_{H_{u,d}}$ and $\tan\beta - A_0$ planes are displayed. Color coding is same as in Fig. 1. The left panels represent $\mu < 0$ and the right panels represent $\mu > 0$ cases. In $m_L - m_R$ plane we see that the left and right panels have almost similar data spread with some minor differences. For example, in the left panel we have more points around $m_R \sim 12$ TeV, while in the right panel the maximum value of $m_L \approx 10$ TeV. In the $\tan\beta - m_{H_{u,d}}$ plane, right panel seems to be more populated in red points as compared to the left panel. We can see that in the right panel red points are $10 \lesssim \tan\beta \lesssim 60$ with $0 \lesssim m_{H_{u,d}} \lesssim 7$ TeV. This apparent difference is due to lack of data in the case of $\mu < 0$. By generating more data, we can reduce the apparent differences. In $\tan\beta - A_0$ plane too, we see the same situation. But one thing is clear from both panels which is that data favours $A_0 < 0$.

Plots in $\mu - \Delta_{EW}$ and $\Delta_{HS} - \Delta_{EW}$ planes are shown in Fig. 4. Color coding is same as in Fig. 1. The top left and right panels depict plots with large ranges of parameters as compared to the bottom left and right panels. Moreover, the left and right panels represent $\mu < 0$ and $\mu > 0$ scenario, respectively. With large parameter ranges, the top two panels almost look like the mirror images of each other. But from the left panel we see that it is relatively easy to have WMAP9 compatible red points with $\mu < 0$ as compared right panel with $\mu > 0$ where the

minimal value of Δ_{EW} for red points is about 2800. In order to investigate further we redraw the same plot with small ranges of parameters. We immediately note that there are some red points below $\Delta_{EW} \lesssim 200$. We also note that the minimal values of Δ_{EW} with and without WMAP9 bounds are 56(1.78% FT) and 24(4.1% FT) respectively. On the other hand in the right panel we see that the minimum value of Δ_{EW} for magenta points is 31(3.2% FT). We have also checked that in the right panel, points with relatively small values of Δ_{EW} have relic density of about 1. This shows that if we try more harder we can get some solutions with small Δ_{EW} and compatible with the WMAP9 bounds. In the bottom left and right panels we show plots in $\Delta_{HS} - \Delta_{EW}$ plane. Here we see that for the entire data $\Delta_{HS} \gtrsim \Delta_{EW}$. We note that for $\mu < 0$ case the minimal value of Δ_{HS} is 1125 (0.08% FT) with Δ_{EW} value of 297(0.33% FT), while we have 963(0.1% FT) and 285(0.35% FT) for Δ_{HS} and Δ_{EW} respectively for $\mu > 0$. It was shown in dedicated studies of natural supersymmetry [62, 63] that with the above definitions of Δ_{EW} and Δ_{HS} it is possible to have values for both the measures $\lesssim 50$ simultaneously.

In Fig. 5 we show graphs in $m_h - \Delta_{EW}$, $m_h - \mu$ and $m_h - m_{3/2}$ planes. Color coding is same as in Fig. 1 with only one exception that there are no magenta color points. In these plots vertical solid black lines represent Higgs mass bounds of 123 GeV and 127 GeV. Here we want to show Δ_{EW}, μ, $m_{3/2}$ and corresponding m_h values. We note that most of our solutions in both the left and right panels are around $m_h \approx$125 GeV. Plots in $m_h - m_{3/2}$ show that the gravitino mass $m_{3/2}$ has to be more than 2 TeV in both cases to have solutions consistent with bounds on Higgs mass 123 to 127 GeV.

We know that the LHC is a color particle producing machine. Among the color particles, gluinos are the smoking guns for the SUSY signals. Recent analysis have put limits of gluino mass $m_{\tilde{g}} \gtrsim 1.7$ TeV (for $m_{\tilde{g}} \sim m_{\tilde{q}}$) and $m_{\tilde{g}} \gtrsim 1.3$ TeV (for $m_{\tilde{g}} \gtrsim m_{\tilde{q}}$) [37, 38]. In Fig. 6 we present plots in $m_{\tilde{g}} - \Delta_{EW}$ and $m_{\tilde{g}} - \mu$ planes. Color coding is same as in Fig. 1 except we do not apply gluino mass bounds mentioned in Section 2. The top left and right panels depict plots with large ranges of parameters as compared to the bottom left and right panels. Moreover, the left and right panels represent $\mu < 0$ and $\mu > 0$ scenario receptively. Here we show that in both scenarios we have heavy gluinos as M_3 is a free parameter in our model. Such solutions can easily evade the above mentioned LHC bounds on gluino and squarks. In top left frame, we see that we have $m_{\tilde{g}} \gtrsim 3$ TeV for small values of Δ_{EW} in case of red points. Interestingly, there exists a region of parameter space with $|\mu| \lesssim 500$ GeV and $\Delta_{EW} \lesssim 300$, where gluino masses are from 3 to 7 TeV, and the first two-generation squarks and sleptons are respectively in the mass ranges [4, 7] TeV and [2, 4] TeV. Because such parameter space is natural from low-energy fine-tuning definition while the gluino and first two-generation squarks/sleptons can not be probed at the 14 TeV LHC, this will provide a strong motivation for 33 TeV and 100 TeV

proton-proton colliders. In the top right frame, we have red points around $m_{\tilde{g}} \sim 5$ TeV with $\Delta_{EW} \sim 2000$. Even if we consider magenta points, we see that we lose very tiny amount of data because of LHC bounds on gluino mass and most of our data remains intact. We also note that in our model Δ_{EW} can be small over the gluino mass range of 2 to 10 TeV (magenta points). It is shown in [64] that the squarks/gluinos of 2.5 TeV, 3 TeV and 6 TeV may be probed by the LHC14, High Luminosity (HL)LHC14 and High Energy (HE) LHC33, respectively. This clearly shows that our models have testable predictions. Moreover, in future if we have collider facility with even higher energy, we will be able to probe over even larger values of sparticle masses.

We present results with neutralino mass verses $\tilde{\tau}_1$, A and $\tilde{\chi}_1^{\pm}$ masses in Fig. 7. Color coding is same as in Fig. 1 and same panel description. Solid black lines are just to guide the eyes, where we can expect to have coannihilation and resonance solutions. In the top left and right panels we have plots in $m_{\tilde{\chi}_1^0} - m_{\tilde{\tau}_1}$ plane. We here note that in the left panel, if do not care about the stringent WMAP9 5σ bounds we have $\tilde{\tau}_1$ nearly degenerate with $\tilde{\chi}_1^0$ from 0.3 TeV to 2.8 TeV. But the solutions satisfy WMAP9 5σ bounds have stau mass in the range of 1.2 TeV to 2.8 TeV. In the right panel, stau mass range is 0.8 TeV to 2.6 TeV while we see the solutions without WMAP9 bonds have the have same stau mass range as we have in the left panel. Here we also note that the next to NLSP (NNLSP) $m_{\tilde{\chi}_1^{\pm}}$ is close to NLSP $m_{\tilde{\tau}}$ in mass. Their masses also lie within the 20% of LSP $\tilde{\chi}_1^0$ mass. In the bottom left and right panels of the figure we present plots in $m_{\tilde{\chi}_1^0} - m_A$ plane. We see that, in both panels we have A-resonance solutions for more than 1 TeV m_A without WMAP9 bounds. But if WMAP9 5σ consistent points have $m_A \gtrsim 2$ TeV.

Graphs in $m_{\tilde{\chi}_1^0} - m_{\tilde{t}_1}$ and $m_{\tilde{\chi}_1^0} - m_{\tilde{g}}$ planes are shown in Fig. 8 with the same color coding and panel description given in Fig. 1, except in middle and bottom panels we do not apply gluino bounds mentioned in Section 2. From top left panel we see that we have two red points compatible with the WMAP9 bounds and representing neutralino-stop coannihilation scenario with mass around 570 GeV and 1.2 TeV respectively. On the other hand in the right panel we do not have red points along the line but we know that it is just because of lack of statistics. In the middle left and right panels we show graphs in $m_{\tilde{\chi}_1^0} - m_{\tilde{g}}$. In both cases we see that there are no WMAP9 compatible red points. But we do note that we have some magenta solutions where gluino and neutralino masses are almost degenerate and $\Omega h^2 < 1$. In the right panel we see only one magenta point near the black line but we can always generate more data around this point. Graphs in the bottom panels show that in our model, we can accommodate gluinos as heavy as 18 TeV consistent with WMAP9 5σ bounds. Such a scenario suggest that there should be very high energy collider in order to probe such model points.

We quantify t-b-τ and b-τ the Yukawa coupling unification (YU) via the R-parameter

$$R_{tb\tau} \equiv \frac{\max(y_t, y_b, y_\tau)}{\min(y_t, y_b, y_\tau)}, R_{b\tau} \equiv \frac{\max(y_b, y_\tau)}{\min(y_b, y_\tau)}, \tag{21}$$

where y_t, y_b and y_τ are Yukawa couplings at the scale of the Grand Unified Theory (GUT). $R_{tb\tau} = 1$ ($R_{b\tau} = 1$) means $y_t = y_b = y_\tau$ ($y_b = y_\tau$) that is a solution with perfect t-b-τ (b-τ) YU.

In Fig. 9 we present graphs in $\tan\beta - R_{tb\tau}$ and $\tan\beta - R_{b\tau}$ planes. Color coding is same as in Fig 1. The left panels represent graphs in $\tan\beta - R_{tb\tau}$ and $\tan\beta - R_{b\tau}$ planes in case of $\mu < 0$ and the right panels represent plots in $\tan\beta - R_{b\tau}$ and $\tan\beta - R_{tb\tau}$ for $\mu > 0$. The horizontal black dashed line represents 10% or better t-b-τ (b-τ) YU. We see in the top left panel that in our scans we have 10% or better YU solutions for $\tan\beta \sim 50 - 60$. The minimal value for $R_{tb\tau}$ we have is 1.05 (5% YU). We note that red points below the dashed line have $m_h \sim 125$ GeV, gluino in the mass range of 8 TeV to 10 TeV, the first two generation squarks and sleptons are in the mass ranges of 8 TeV to 9.5 TeV and 3 TeV 3.5 TeV respectively. The third generation squarks and sleptons lie in the mass ranges of 5 TeV to 7.5 TeV and 1.3 TeV to 3 TeV. They also have large values for $|\mu|$ ($\sim$ -5 TeV to -4 TeV) and $\Delta_{EW} \sim$ 4000 to 8500. More or less magenta points also have the similar mass spectrum. It was shown in more exhausted studies (see e.g [65] and references there in) with non-universal gaugino masses that one can have 100% YU with the LHC testable predictions.

In the bottom left panel we have b-τ YU solutions. Since this is a less constraint situation, we have 10% or better YU solutions for a wider range of $\tan\beta$, *i.e.*, $30 \lesssim \tan\beta \lesssim 60$. Here, the minimal value of $R_{b\tau}$ is about 1.04 (4% YU). Moreover, the particle mass spectra also have slightly wider ranges as compared to t-b-τ YU case. We also note that those magenta points, which do not satisfy WMAP9 bounds, have more or less the same mass ranges as given above.

In the top right panel, we see that we do not have even magenta solution with 10% or better t-b-τ YU with $\mu > 0$. It was noticed that in a SUSY $SO(10)$ GUT with non-universal SSB gaugino masses at $M_{\rm GUT}$ and $\mu > 0$, t-b-τ Yukawa unification [66] can lead one to predict the lightest CP even Higgs boson mass to be 125 GeV [67]. Even if we consider gaugino-universality 10% or better t-b-τ YU can be achieved consistent with the LHC bounds [68] but very hard to satisfy relic density bounds. In our scans, we have solutions with 12% t-b-τ YU, if we do dedicated searches for better YU solutions, we can get them. Since here, we are not so keen to have 100% YU solutions but to give a flavor that our model can admit such solutions. In the bottom right panel we see that we have only three red points. On the other hand we have plenty of magenta points with 10% or better b-τ YU. In fact, we have $R_{b\tau}$ =1, *i.e.*, 100% b-τ YU solutions for $\tan\beta \sim$ 30-55. In order to save such solutions we have to add some extra physics to the MSSM. In such scenario we can consider SUSY models augmented with Peccei-Quinn(PQ)

solution to the strong CP problem [69] (PQMSSM). In SUSY context the axino field is just one element of an axion supermultiplet. The axion supermutiplet contains a complex scalar field, whose real part is the R-parity even saxion field $s(x)$ and whose imaginary part is the axion field $a(x)$. The supermutliplet also contains an R-parity odd spin half Majorana field, the axino $\tilde{a}(x)$[70]. In case where $\Omega h^2 \gtrsim 1$, one way to have relic density within the observed range if we assume the $\tilde{\chi}_1^0$ may not be the LSP, but instead decays to much lighter state, such as $\tilde{\chi}_1^0 \to \gamma\tilde{a}$, where $\tilde{a}$ is axino. In such a scenario we have mixed axion/axino ($a\tilde{a}$) dark matter [71]. In this way the neutralino abundance is converted into an axino abundance with [72]

$$\Omega_{\tilde{a}} h^2 = \frac{m_{\tilde{a}}}{m_{\tilde{\chi}_1^0}} \Omega^2_{\tilde{\chi}_1^0}. \tag{22}$$

It is important to know the life time (τ) of decaying neutralino. If it is more than 1 second, it can disturb Big Bang Nucleosynthesis (BBN) (see [73] and references there in). We first calculate $m_{\tilde{a}}$ for a given $m_{\tilde{\chi}_1^0}$ and its relic density $\Omega^2_{\tilde{\chi}_1^0}$ by assuming relic density of axino $\Omega_{\tilde{a}} h^2$ =0.11 by using Eq. 22. We then follow [74] to calculate the lifetime for the decaying NLSP neutralino. We use $C_{aYY} = 8/3$ in the DFSZ model [75], N =6 (the color anomaly model dependent factor). We present our calculations in Fig. 10, where we display the NLSP bino-like neutralino mass ($m_{\tilde{\chi}_1^0}$) versus its lifetime (τ). Panel description is same as in Fig. 1. Here points in various colors correspond to various choices of the axion decay constant f_a values. The light-green, light-blue, orange, black, dark-green and blue represent $f_a = 10^{10} - 10^{15}$ GeV, respectively. The black solid line show τ =1 second. In the left panel, the plot appears somewhat flat as compare to the right plot in right panel because of small mass range. From both the frames, it is clearly visible that for $f_a = 10^{15}$ GeV, life time of NLSP bino is more than 1 second. For $f_a = 10^{14}$ GeV, in the right panel, points with bino mass greater than 1 TeV are allowed.

In another approach to reduce relic density is to assume the additional late decaying scalar fields are present in the model. These fields may get produced at large rates via coherent oscillations. If they temporarily dominate the energy density of the Universe, and then decay to mainly SM particles, they may inject considerable entropy into the cosmic soup, thus diluting all relics which are present at the time of decay. Entropy injection can occur at large rates for instance from saxion production in the PQMSSM [76, 77], or from moduli production and decay, as is expected in string theory [78]. However, it was shown in [79] that the efforts to dilute the relic density of neutralino below the observed dark matter relic density through entropy injection from saxion decays such as saxion decays to gluon violate the CMB bound on ΔN_{eff}, where ΔN_{eff} is the apparent number of additional effective neutrinos.

On the other hand, the solutions with good YU may also have small relic density $\Omega h^2 \sim 10^{-5}$–10^{-2}. In such cases the neutralino abundance can be augmented in the PQMSSM case where

$m_{\tilde{a}} > m_{\tilde{\chi}_1^0}$ and additional neutralinos are produced via thermal axino production and decay $m_{\tilde{a}} \to m_{\tilde{\chi}_1^0}\gamma$ [77]. In these cases, the CDM tends to be neutralino dominated with a small component of axions.

In Fig. 11 we show graphs in $m_{\tilde{\chi}_1^0} - m_{\tilde{\chi}_1^\pm}$ plane with the same panel description as in Fig. 1. The top left and right frames have same color coding as in Fig. 1. From these frames, it is apparent that we have solutions from 0.1 TeV to 2.8 TeV. In bottom frames we further analyse these points on the basis of neutralino composition. Here orange, green and brown points represent neutralino with more than 90% wino, more than 80% bino and more than 50% higgsino composition, respectively. It is to be noted that orange and the green points satisfy all constraints given Section 2 but brown point do not satisfy relic density bounds. Here, we want to show that in our scans where the neutralino and chargino masses are almost degenerate, and neutralino LSP can be of bino, wino and higgsino like. We immediately see that in both cases ($\mu < 0$ and $\mu > 0$), wino-type neutralino have masses more than 1 TeV. On the other hand bino-like solutions have masses less than 1 TeV while higgsino-type solutions have mass range of 150 to 600 GeV. It is shown in [39, 40] that for NFW and Einasto distribution, the entire mass range of thermal wino dark matter from 0.1 to 3 TeV may be excluded. In a recent study [80], wino as dark matter candidate is excluded in the mass range bellow 800 GeV from antiproton and between 1.8 TeV to 3.5 TeV from the absence of a γ-ray line feature toward the galactic center. Since our bino-like points have some admixture of higgsinos and that is why they have large nucleon-neutralino scattering cross section. Such solutions are also under stress because of the current upper bound set by XENON100 [81]. Here, we argue that such wino-like (bino-like) neutralino solutions may avoid the above mentioned bounds. For example, the wino-like neutralino density is smaller than the observed density. Otherwise, instead of treating them as the LSPs we assume that they are the NLSP and may decay to axino and γ as we have discussed above. Similarly, we can also assume the mechanism of late decaying fields via coherent oscillations or production of moduli and their decay as we argued previously. In addition to it, we can also invoke R-parity violation scenario, where the bino LSP and similarly wino-like neutralino can decay to the SM fermions via sfermion exchange. In order to address the issue of underabundance of higgsino-like solutions we argue that mainly higgsino-like neutralino by itself does not make a good cold dark matter candidate and we need additional dark matter candidates to match the observed dark matter relic density. For this purpose we assume that the higgsino could make up only a fraction of the relic dark matter and the remaining abundance is comprised of axions produces through the vacuum misalignment mechanism [83]. This is why we could expect the higgsino relic density somewhat suppressed between $1 - 15$ in the present universe. This not only provides us with the opportunity to look

for higgsinos, despite the fact that they would only constitute a fraction of the measured relic dark matter abundance but also the possibility to detect axions. We would also like to mention that our higgsino-like solutions especially for $\Delta_{EW} \lesssim 50$ more or less look like the solutions form radiative natural SUSY [84]. Since such solutions tend to have large direct and indirect neutralino detection rates, let us check the status of our higgsino-like solutions. We will follow [85]. In the left panel of Fig. 12 we plot rescaled higgsino-like neutralino spin-independent cross section $\xi\sigma^{SI}(\tilde{Z}_1 p)$ versus m(higgsino) (in this figure for both panels we have combined solutions with $\mu < 0$ and $\mu > 0$). The orange solid line represents the current upper bound set by the CDMS experiment and black solid line depicts upper bound set by XENON100 [81], while the orange (black) dashed line represents future reach of SuperCDMS [86] (XENON1T [87]). We rescale our result by a factor $\xi = \Omega_{\tilde{Z}_1} h^2/0.11$ in order to account for the fact that the local relic density might be much less than the usually assumed value $\rho_{local} \simeq 0.3\,\mathrm{GeV}/cm^3$ as pointed out in [88]. Here, we see that all the points lie below the current upper bounds set by CDMS XENON100 experiments. It is very clear that the future experiments like XENON1T will be able to probe almost all of our model points. This shows our results are in agreement with [85] where it was shown that all higgsino points could be tested by the XENON1T and one could discover neutralino (WIMPs) or exclude the concept of electroweak naturalness in R-parity conserving natural SUSY models. In right panel of Fig. 12, we have a plot of (non-rescaled) higgsino-like neutralino spin-dependent cross section $\sigma^{SD}(\tilde{Z}_1 p)$ versus m(higgsino). The IceCube DeepCore and future IceCube DeepCore bounds are shown in black solid line and black dashed line [89]. Color coding is same as in left panel. Here we do not rescale our results because the IceCube detection depends on whether the Sun has equilibrated its core abundance between capture rate and annihilate rate [90]. It was shown in [91] that for the Sun, equilibrium is reached for almost all of SUSY parameter space. In this plot we see that the future IceCube DeepCore searches will be able to probe our entire set of solutions in our present scans.

In Tables 1-3, we list benchmark points for $\mu < 0$ case. All of these points satisfy the sparticle mass, B-physics and Higgs mass constraints described in Section 2. In Table 1, point 1(2) represents the minimal value of Δ_{EW} not consistent and consistent with WMAP9 5σ bounds, while points 3-5 respectively correspond to the minimal value of Δ_{HS}, best point with t-b-τ and b-τ YU, an example of heavy gluino solution. Points 3 and 4 also satisfy WMAP9 5σ bounds. In Table 2, points 1, 2, 3 and 4 display neutralino-stau, neutralino-stop, m_A-resonance and neutralino-gluino coannihilation, respectively. Point 4 is the case where relic density is below WMAP9 5σ bounds. In Table 3, point 1 represents bino-like neutralino, point 2 displays higgsino like neutralino, point 3 and point 4 are examples of wino-like neutralino. Point 2 and point 4 do not satisfy WMAP9 5σ bounds.

In Tables 4-6, we display benchmark points for $\mu > 0$ case consistent with the sparticle mass, B-physics and Higgs mass constraints described in Section 2. In Table 4, points 1-4 respectively correspond to the minimal value of Δ_{EW}, minimal value of Δ_{HS}, best point with b-τ YU, an example of heavy gluino solution. Points 3 and 4 also satisfy WMAP9 5σ bounds. Table 5 and Table 6 have similar description as Table 2 and Table 3.

5 Discussions and Conclusion

The three-family Pati-Salam models have been constructed systematically in Type IIA string theory on the $\mathbf{T^6}/(\mathbb{Z}_\mathbf{2} \times \mathbb{Z}_\mathbf{2})$ orientifold with intersecting D6-branes [16]. It was found that one model has a realistic phenomenology [33, 34]. Considering the Higgs boson mass around 125 GeV and the LHC supersymmetry search constraints, we have revisited this three-family Pati-Salam model in details. We systematically scanned the viable parameter space for $\mu < 0$ and $\mu > 0$, and found that in general the gravitino mass is heavier than about 2 TeV for both cases because of the Higgs boson mass low bound 123 GeV. In particular, we identified a natural region of parameter space where the electroweak fine-tuning can be as small as $\Delta_{EW} \sim$ 24-32 (3-4%). Also, we found another interesting region of parameter space with $|\mu| \lesssim 500$ GeV and $\Delta_{EW} \lesssim 300$, where the mass ranges for the gluino, and first two-generation squarks and sleptons are [3, 7] TeV, [4, 7] TeV, and [2, 4] TeV, respectively. This will provide a strong motivation for 33 TeV and 100 TeV proton-proton colliders since it is natural from low-energy fine-tuning definition while the gluino and first two generation squarks/sleptons are heavy. In the whole viable parameter space which is consistent with all the current experimental constraints including the dark matter relic density bounds, the gluino mass range is [3, 18] TeV, the first two-family squarks have masses from 3 to 16 TeV, and the first two-family sleptons have masses from 2 to 7 TeV. Thus, the viable parameter space with heavy gluino and squarks is even out of reach of the 100 TeV proton collider [92]. On the other hand, for the third-family sfermions, the NLSP light stop satisfying 5σ WMAP bounds is in the mass range [0.5, 1.2] TeV, and the light stau can be as light as 800 GeV. We also showed various coannihilation and resonance scenarios through which the observed dark matter relic density can be achieved. Interestingly, the certain portions of parameter space have excellent t-b-τ and b-τ Yukawa coupling unification. Also, we highlighted the regions of parameter space where the LSP neutralino can be a bino, wino, or higgsino. We discussed various scenarios in which such solutions may avoid recent astrophysical bounds in case if they satisfy or above the correct dark matter relic density bounds. Prospects of finding higgsino-like neutralino in direct and indirect searches were shown and discussed as well. To be concrete, we displayed six benchmark tables depicting various interesting features of our model. Furthermore, because the LSP neutralino

can be heavier than 1 TeV and up to about 2.8 TeV, how to test such scenario at the 14 TeV LHC is still a big question. Therefore, the 33 TeV and 100 TeV proton-proton colliders are indeed needed to probe our D-brane model.

Acknowledgements

We would like to thank Howard Baer, Eung-Jin Chun, Bin He, and Azar Mustafayev very much for helpful discussions. The work of TL, SR and XW is supported in part by by the Natural Science Foundation of China under grant numbers 10821504, 11075194, 11135003, and 11275246, and by the National Basic Research Program of China (973 Program) under grant number 2010CB833000. And the work of DVN was supported in part by the DOE grant DE-FG03-95-ER-40917.

References

[1] W. Buchmuller, K. Hamaguchi, O. Lebedev and M. Ratz, Phys. Rev. Lett. **96**, 121602 (2006), and references therein.

[2] O. Lebedev, H. P. Nilles, S. Raby, S. Ramos-Sanchez, M. Ratz, P. K. S. Vaudrevange and A. Wingerter, Phys. Lett. B **645**, 88 (2007), and references therein.

[3] J. E. Kim and B. Kyae, Nucl. Phys. B **770**, 47 (2007); Phys. Rev. D **77**, 106008 (2008); J. H. Huh, J. E. Kim and B. Kyae, arXiv:0904.1108 [hep-ph].

[4] V. Braun, Y. H. He, B. A. Ovrut and T. Pantev, Phys. Lett. B **618**, 252 (2005); JHEP **0605**, 043 (2006), and references therein.

[5] V. Bouchard and R. Donagi, Phys. Lett. B **633**, 783 (2006), and references therein.

[6] I. Antoniadis, J. R. Ellis, J. S. Hagelin and D. V. Nanopoulos, Phys. Lett. B **205** (1988) 459; Phys. Lett. B **208** (1988) 209 [Addendum-ibid. B **213** (1988) 562]; Phys. Lett. B **231** (1989) 65.

[7] A. E. Faraggi, D. V. Nanopoulos and K. J. Yuan, Nucl. Phys. B **335**, 347 (1990).

[8] I. Antoniadis, G. K. Leontaris and J. Rizos, Phys. Lett. B **245**, 161 (1990).

[9] J. L. Lopez, D. V. Nanopoulos and K. J. Yuan, Nucl. Phys. B **399**, 654 (1993); D. V. Nanopoulos, hep-ph/0211128.

[10] G. B. Cleaver, A. E. Faraggi, D. V. Nanopoulos and J. W. Walker, Nucl. Phys. B **620**, 259 (2002), and references therein.

[11] M. Berkooz, M. R. Douglas and R. G. Leigh, Nucl. Phys. B **480**, 265 (1996).

[12] L. E. Ibanez, F. Marchesano and R. Rabadan, JHEP **0111**, 002 (2001).

[13] R. Blumenhagen, B. Kors, D. Lust and T. Ott, Nucl. Phys. B **616**, 3 (2001).

[14] M. Cvetič, G. Shiu and A. M. Uranga, Phys. Rev. Lett. **87**, 201801 (2001); M. Cvetič, G. Shiu and A. M. Uranga, Nucl. Phys. B **615**, 3 (2001).

[15] M. Cvetič, I. Papadimitriou and G. Shiu, Nucl. Phys. B **659**, 193 (2003) [Erratum-ibid. B **696**, 298 (2004)].

[16] M. Cvetic, T. Li and T. Liu, Nucl. Phys. B **698**, 163 (2004) [hep-th/0403061].

[17] M. Cvetic, P. Langacker, T. Li and T. Liu, Nucl. Phys. B **709**, 241 (2005) [hep-th/0407178].

[18] M. Cvetic, T. Li and T. Liu, Phys. Rev. D **71**, 106008 (2005) [hep-th/0501041].

[19] C.-M. Chen, G. V. Kraniotis, V. E. Mayes, D. V. Nanopoulos and J. W. Walker, Phys. Lett. B **611**, 156 (2005); Phys. Lett. B **625**, 96 (2005).

[20] C. M. Chen, T. Li and D. V. Nanopoulos, Nucl. Phys. B **732**, 224 (2006).

[21] R. Blumenhagen, M. Cvetic, P. Langacker and G. Shiu, Ann. Rev. Nucl. Part. Sci. **55**, 71 (2005), and references therein.

[22] T. P. T. Dijkstra, L. R. Huiszoon and A. N. Schellekens, Phys. Lett. B **609**, 408 (2005).

[23] T. P. T. Dijkstra, L. R. Huiszoon and A. N. Schellekens, Nucl. Phys. B **710**, 3 (2005), and references therein.

[24] C. Vafa, Nucl. Phys. B **469**, 403 (1996).

[25] R. Donagi and M. Wijnholt, arXiv:0802.2969 [hep-th].

[26] C. Beasley, J. J. Heckman and C. Vafa, JHEP **0901**, 058 (2009).

[27] C. Beasley, J. J. Heckman and C. Vafa, JHEP **0901**, 059 (2009).

[28] R. Donagi and M. Wijnholt, arXiv:0808.2223 [hep-th].

[29] A. Font and L. E. Ibanez, JHEP **0902**, 016 (2009) [arXiv:0811.2157 [hep-th]].

[30] J. Jiang, T. Li, D. V. Nanopoulos and D. Xie, Phys. Lett. B **677**, 322 (2009).

[31] J. Jiang, T. Li, D. V. Nanopoulos and D. Xie, Nucl. Phys. B **830**, 195 (2010) [arXiv:0905.3394 [hep-th]].

[32] T. Li, Phys. Rev. D **81**, 065018 (2010) [arXiv:0905.4563 [hep-th]].

[33] C. -M. Chen, T. Li, V. E. Mayes and D. V. Nanopoulos, Phys. Lett. B **665**, 267 (2008) [hep-th/0703280].

[34] C. -M. Chen, T. Li, V. E. Mayes and D. V. Nanopoulos, Phys. Rev. D **77**, 125023 (2008) [arXiv:0711.0396 [hep-ph]].

[35] G. Aad *et al.* [ATLAS Collaboration], Phys. Lett. B **716**, 1 (2012) [arXiv:1207.7214 [hep-ex]].

[36] S. Chatrchyan *et al.* [CMS Collaboration], Phys. Lett. B **716**, 30 (2012) [arXiv:1207.7235 [hep-ex]].

[37] S. Chatrchyan *et al.* [CMS Collaboration], Phys. Lett. B **725**, 243 (2013) [arXiv:1305.2390 [hep-ex]].

[38] G. Aad *et al.* [ATLAS Collaboration], arXiv:1405.7875 [hep-ex].

[39] J. Fan and M. Reece, JHEP **1310**, 124 (2013) [arXiv:1307.4400 [hep-ph]].

[40] T. Cohen, M. Lisanti, A. Pierce and T. R. Slatyer, JCAP **1310**, 061 (2013) [arXiv:1307.4082].

[41] H. Baer, F. E. Paige, S. D. Protopopescu and X. Tata, arXiv:hep-ph/0001086.

[42] J. Hisano, H. Murayama, and T. Yanagida, Nucl. Phys. **B402** (1993) 46. Y. Yamada, Z. Phys. **C60** (1993) 83; J. L. Chkareuli and I. G. Gogoladze, Phys. Rev. D **58**, 055011 (1998).

[43] D. M. Pierce, J. A. Bagger, K. T. Matchev, and R.-j. Zhang, Nucl. Phys. **B491** (1997) 3.

[44] L. E. Ibanez and G. G. Ross, Phys. Lett. **B110** (1982) 215; K. Inoue, A. Kakuto, H. Komatsu and S. Takeshita, Prog. Theor. Phys. **68**, 927 (1982) [Erratum-ibid. **70**, 330 (1983)]; L. E. Ibanez, Phys. Lett. **B118** (1982) 73; J. R. Ellis, D. V. Nanopoulos, and K. Tamvakis,

Phys. Lett. **B121** (1983) 123; L. Alvarez-Gaume, J. Polchinski, and M. B. Wise, Nucl. Phys. **B221** (1983) 495.

[45] J. Beringer *et al.* [Particle Data Group Collaboration], Phys. Rev. D **86**, 010001 (2012).

[46] [Tevatron Electroweak Working Group and CDF Collaboration and D0 Collab], arXiv:0903.2503 [hep-ex].

[47] I. Gogoladze, R. Khalid, S. Raza and Q. Shafi, JHEP **1106** (2011) 117.

[48] G. Belanger, F. Boudjema, A. Pukhov and R. K. Singh, JHEP **0911**, 026 (2009); H. Baer, S. Kraml, S. Sekmen and H. Summy, JHEP **0803**, 056 (2008).

[49] H. Baer and M. Brhlik, *Phys. Rev.* **D 55** (1997) 4463; H. Baer, M. Brhlik, D. Castano and X. Tata, *Phys. Rev.* **D 58** (1998) 015007;

[50] K. Babu and C. Kolda, *Phys. Rev. Lett.* **84** (2000) 228; A. Dedes, H. Dreiner and U. Nierste, *Phys. Rev. Lett.* **87** (2001) 251804; J. K. Mizukoshi, X. Tata and Y. Wang, *Phys. Rev.* **D 66** (2002) 115003.

[51] D. Eriksson, F. Mahmoudi and O. Stal, *J. High Energy Phys.* **0811** (2008) 035.

[52] R. Aaij *et al.* [LHCb Collaboration], Phys. Rev. Lett. **110**, 021801 (2013).

[53] Y. Amhis *et al.* [Heavy Flavor Averaging Group Collaboration], arXiv:1207.1158 [hep-ex].

[54] D. Asner *et al.* [Heavy Flavor Averaging Group Collaboration], arXiv:1010.1589 [hep-ex].

[55] G. Aad *et al.* [ATLAS Collaboration], Phys. Lett. B **716**, 1 (2012).

[56] S. Chatrchyan *et al.* [CMS Collaboration], Phys. Lett. B **716**, 30 (2012); arXiv:1303.4571 [hep-ex].

[57] G. Hinshaw *et al.* [WMAP Collaboration], arXiv:1212.5226 [astro-ph.CO].

[58] H. Baer, V. Barger, P. Huang, D. Mickelson, A. Mustafayev and X. Tata, Phys. Rev. D **87**, no. 3, 035017 (2013) [arXiv:1210.3019 [hep-ph]].

[59] J. R. Ellis, K. Enqvist, D. V. Nanopoulos and F. Zwirner, Mod. Phys. Lett. A **1**, 57 (1986).

[60] R. Barbieri and G. F. Giudice, Nucl. Phys. B **306**, 63 (1988).

[61] H. Baer, V. Barger, P. Huang, A. Mustafayev and X. Tata, Phys. Rev. Lett. **109**, 161802 (2012) [arXiv:1207.3343 [hep-ph]].

[62] I. Gogoladze, F. .Nasir and Q. .Shafi, Int. J. Mod. Phys. A **28**, 1350046 (2013) [arXiv:1212.2593 [hep-ph]].

[63] I. Gogoladze, F. Nasir and Q. Shafi, JHEP **1311**, 173 (2013) [arXiv:1306.5699 [hep-ph]].

[64] **CMS** Collaboration, "CMS at the High-Energy Frontier Contribution to the Update of the European Strategy for Particle Physics." [CMS-NOTE-2012-006]

[65] I. Gogoladze, R. Khalid, S. Raza and Q. Shafi, JHEP **1012**, 055 (2010) [arXiv:1008.2765 [hep-ph]]. I. Gogoladze, R. Khalid, S. Raza and Q. Shafi, JHEP **1106**, 117 (2011) [arXiv:1102.0013 [hep-ph]]. I. Gogoladze, Q. Shafi and C. S. Un, Phys. Lett. B **704**, 201 (2011) [arXiv:1107.1228 [hep-ph]]. I. Gogoladze, Q. Shafi and C. S. Un, JHEP **1207**, 055 (2012) [arXiv:1203.6082 [hep-ph]].

[66] B. Ananthanarayan, G. Lazarides and Q. Shafi, Phys. Rev. D **44**, 1613 (1991); Phys. Lett. B **300**, 24 (1993); Q. Shafi and B. Ananthanarayan, Trieste HEP Cosmol. 1991:233-244.

[67] I. Gogoladze, Q. Shafi and C. S. Un, JHEP **1208**, 028 (2012); M. Adeel Ajaib, I. Gogoladze, Q. Shafi and C. S. Un, JHEP **1307**, 139 (2013). M. A. Ajaib, I. Gogoladze, Q. Shafi and C. S. n, JHEP **1405**, 079 (2014) [arXiv:1402.4918 [hep-ph]].

[68] H. Baer, S. Raza and Q. Shafi, Phys. Lett. B **712**, 250 (2012) [arXiv:1201.5668 [hep-ph]].

[69] R. Peccei and H. Quinn, *Phys. Rev. Lett.* **38** (1977) 1440 and *Phys. Rev.* **D 16** (1977) 1791; S. Weinberg, *Phys. Rev. Lett.* **40** (1978) 223; F. Wilczek, *Phys. Rev. Lett.* **40** (1978) 279.

[70] H. P. Nilles and S. Raby, Nucl. Phys. B **198** (1982) 102; J. E. Kim, Phys. Lett. B **136** (1984) 378; J. E. Kim and H. P. Nilles, Phys. Lett. B **138** (1984) 150; for a review, see *e.g.* F. D. Steffen, Eur. Phys. J. C **59** (2009) 557.

[71] H. Baer and H. Summy, *Phys. Lett.* **B 666** (2008) 5; H. Baer, M. Haider, S. Kraml, S. Sekmen and H. Summy, JCAP**0902** (2009) 002.

[72] L. Covi, J. E. Kim and L. Roszkowski, *Phys. Rev. Lett.* **82** (1999) 4180; L. Covi, H. B. Kim, J. E. Kim and L.Roszkowski, *J. High Energy Phys.* **0105** (2001) 033.

[73] K. -Y. Choi, J. E. Kim and L. Roszkowski, J. Korean Phys. Soc. **63**, 1685 (2013) [arXiv:1307.3330 [astro-ph.CO]].

[74] H. Baer, S. Kraml, A. Lessa and S. Sekmen, JCAP **1011**, 040 (2010) [arXiv:1009.2959 [hep-ph]].

[75] M. Dine, W. Fischler and M. Srednicki, Phys. Lett. B **104**, 199 (1981). A. R. Zhitnitsky, Sov. J. Nucl. Phys. **31**, 260 (1980) [Yad. Fiz. **31**, 497 (1980)].

[76] G. Lazarides, C. Panagiotakapolous and Q. Shafi, *Phys. Lett.* **B 192** (1987) 323;G. Lazarides, R. Schaefer, D. Seckel and Q. Shafi, *Nucl. Phys.* **B 346** (1990) 193;J. McDonald, *Phys. Rev.* **D 43** (1991) 1063; C. Pallis, *Astropart. Phys.* **21** (2004) 689.

[77] K-Y. Choi, J. E. Kim, H. M. Lee and O. Seto, *Phys. Rev.* **D 77** (2008) 123501; H. Baer, S. Kraml, A. Lessa and S. Sekmen, JCAP **1104** (2011) 039; H. Baer and A. Lessa, *J. High Energy Phys.* **1106** (2011) 027; H. Baer, A. Lessa, S. Rajagopalan and W. Sreethawong, JCAP**1106** (2011) 031; H. Baer, A. Lessa and W. Sreethawong, JCAP **1201**, 036 (2012)

[78] T. Moroi and L. Randall, *Nucl. Phys.* **B 570** (2000) 455; G. Gelmini and P. Gondolo, *Phys. Rev.* **D 74** (2006) 023510; G. Gelmini, P. Gondolo, A. Soldatenko and C. Yaguna, *Phys. Rev.* **D 74** (2006) 083514; G. Gelmini, P. Gondolo, A. Soldatenko and C. Yaguna, *Phys. Rev.* **D 76** (2007) 015010; B. Acharya, K. Bobkov, G. Kane, P. Kumar and J. Shao, *Phys. Rev.* **D 76** (2007) 126010 and *Phys. Rev.* **D 78** (2008) 065038; B. Acharya, P. Kumar, K. Bobkov, G. Kane, J. Shao and S. Watson, *J. High Energy Phys.* **0806** (2008) 064.

[79] K. J. Bae, H. Baer and A. Lessa, JCAP **1304**, 041 (2013) [arXiv:1301.7428 [hep-ph]].

[80] A. Hryczuk, I. Cholis, R. Iengo, M. Tavakoli and P. Ullio, arXiv:1401.6212 [astro-ph.HE].

[81] E. Aprile *et al.* [XENON100 Collaboration], Phys. Rev. Lett. **109**, 181301 (2012) [arXiv:1207.5988 [astro-ph.CO]].

[82] S. P. Martin, In *Kane, G.L. (ed.): Perspectives on supersymmetry II* 1-153 [hep-ph/9709356].

[83] L. F. Abbott and P. Sikivie, *Phys. Lett.* **B 120** (1983) 133; J. Preskill, M. Wise and F. Wilczek, *Phys. Lett.* **B 120** (1983) 127; M. Dine and W. Fischler, *Phys. Lett.* **B 120** (1983) 137; M. Turner, *Phys. Rev.* **D 33** (1986) 889; L. Visinelli and P. Gondolo, *Phys. Rev.* **D 80** (2009) 035024.

[84] H. Baer, V. Barger, P. Huang, D. Mickelson, A. Mustafayev and X. Tata, Phys. Rev. D **87**, no. 11, 115028 (2013) [arXiv:1212.2655 [hep-ph]].

[85] H. Baer, V. Barger and D. Mickelson, Phys. Lett. B **726**, 330 (2013) [arXiv:1303.3816 [hep-ph]].

[86] P. L. Brink *et al.* [CDMS-II Collaboration], eConf C **041213**, 2529 (2004) [astro-ph/0503583].

[87] E. Aprile [XENON1T Collaboration], arXiv:1206.6288 [astro-ph.IM].

[88] A. Bottino, F. Donato, N. Fornengo and S. Scopel, Phys. Rev. D **63**, 125003 (2001) [hep-ph/0010203].

[89] R. Abbasi *et al.* [ICECUBE Collaboration], Phys. Rev. Lett. **102**, 201302 (2009) [arXiv:0902.2460 [astro-ph.CO]].

[90] G. Jungman, M. Kamionkowski and K. Griest, Phys. Rept. **267**, 195 (1996) [hep-ph/9506380].

[91] V. Niro, A. Bottino, N. Fornengo and S. Scopel, Phys. Rev. D **80**, 095019 (2009) [arXiv:0909.2348 [hep-ph]].

[92] T. Cohen, T. Golling, M. Hance, A. Henrichs, K. Howe, J. Loyal, S. Padhi and J. G. Wacker, arXiv:1311.6480 [hep-ph].

	Point 1	Point 2	Point 3	Point 4	Point 5
m_L	2763.6	4077.8	1353.6	3125.3	2599.1
m_R	2187.1	3343.4	1401.1	1414.8	4991.8
M_1	-379.47	-441.48	-865.62	4894.5	5792.8
M_2	2850.2	3957.4	-2681.8	1802.4	2082.9
M_3	1495.1	2206.2	-1194.1	4953.4	8736.4
A_0	-3144.2	-5006.1	2127.6	-2884.4	-2626.3
$\tan\beta$	12.8	23	11.1	57.7	46.8
$m_{H_u} = m_{H_d}$	3470	5127.6	1857	1778.4	3692.7
μ	-290	-244	-1110	-5500	-8688
Δ_{EW}	24	56	297	7279	18163
Δ_{HS}	2941	6395	1125	7663	20667
m_h	124	125	123	125	126
m_H	3828	5146	2712	1369	6761
m_A	3803	5112	2695	1360	6717
$m_{H^\pm}$	3828	5146	2713	1373	6762
$m_{\tilde{\chi}^0_{1,2}}$	177, 300	202, 255	377, 1120	1503, 2221	1697, 2647
$m_{\tilde{\chi}^0_{3,4}}$	310, 2375	273, 3314	1122, 2209	5403, 5403	8561, 8561
$m_{\tilde{\chi}^\pm_{1,2}}$	285, 2348	238, 3274	1139, 2193	1506, 5356	1700, 8478
$m_{\tilde{g}}$	3281	4725	2630	9818	16760
$m_{\tilde{u}_{L,R}}$	4239, 3490	6112, 5133	3069, 2626	8934, 8510	14308, 15024
$m_{\tilde{t}_{1,2}}$	1240, 3536	1933, 4958	1273, 2620	6955, 7659	12604, 12906
$m_{\tilde{d}_{L,R}}$	4240, 3491	6112, 5136	3070, 2622	8934, 8456	14308, 14994
$m_{\tilde{b}_{1,2}}$	3386, 3579	4751, 5025	2565, 2638	7066, 7617	12672, 13902
$m_{\tilde{\nu}_{1,2}}$	3294	4767	2175	3415	3015
$m_{\tilde{\nu}_3}$	3268	4624	2162	3221	2551
$m_{\tilde{e}_{L,R}}$	3291, 2187	4763, 3342	2176, 1435	3423, 2273	3006, 5410
$m_{\tilde{\tau}_{1,2}}$	2094, 3264	2898, 4620	1386, 2161	1511, 3218	2527, 4810
σ_{SI}(pb)	2.41×10^{-9}	8.34×10^{-9}	5.97×10^{-11}	2.78×10^{-12}	5.52×10^{-13}
σ_{SD}(pb)	3.39×10^{-5}	1.29×10^{-4}	8.55×10^{-8}	1.52×10^{-9}	1.71×10^{-10}
$\Omega_{CDM}h^2$	0.731	0.101	21.3	0.126	0.115
$R_{tb\tau}$	7.44	4.04	8.68	1.05	1.85
$R_{b\tau}$	1.35	1.35	1.36	1.04	1.35

Table 1: All the masses are in units of GeV and $\mu < 0$. All points satisfy the sparticle mass bounds, and B-physics constraints described in Section 2. Points 1 and 2 represent the minimal value of Δ_{EW} not consistent and consistent with the WMAP9 5σ bounds, while points 3-5 correspond respectively to the minimal value of Δ_{HS}, best points with t-b-τ and b-τ YU, an example of heavy gluino solution. Points 3 and 4 also satisfy the WMAP9 5σ bounds.

	Point 1	Point 2	Point 3	Point 4
m_L	2608.7	4050.1	3521.9	6589.5
m_R	2270.8	2651.8	3022.8	6501
M_1	-4372.3	-2542.1	-4090.1	-2646.7
M_2	-2924.2	-3947.6	-2720.5	-6538.3
M_3	-5426.5	-1767.6	-4397.9	-487.58
A_0	2123.4	4103.5	4070.6	6423.1
$\tan\beta$	33.6	23.5	45.8	32.6
$m_{H_u} = m_{H_d}$	2216.6	3258.7	3615	4428.1
μ	-5691	-2418	-4801	-3572
Δ_{EW}	7793	1489	5546	3070
Δ_{HS}	8745	4049	8489	7761
m_h	126	127	126	125
m_H	5307	4246	3827	5267
m_A	5272	4218	3802	5233
$m_{H^\pm}$	5308	4247	3828	5267
$m_{\tilde{\chi}^0_{1,2}}$	1958, 2437	1155, 2425	1863, 2285	1237, 3591
$m_{\tilde{\chi}^0_{3,4}}$	5718, 5720	2429, 3327	4815, 4817	3592, 5542
$m_{\tilde{\chi}^\pm_{1,2}}$	2444, 5719	2467, 3303	2289, 4817	3646, 5501
$m_{\tilde{g}}$	10673	3847	8807	1308
$m_{\tilde{u}_{L,R}}$	9526, 9362	5644, 4153	8369, 8082	7717, 6555
$m_{\tilde{t}_{1,2}}$	7694, 8601	1186, 4747	6173, 7097	3084, 6172
$m_{\tilde{d}_{L,R}}$	9527, 9324	5645, 4120	8369, 8046	7717,6533
$m_{\tilde{b}_{1,2}}$	8562, 8820	3751, 4817	7022, 7081	5649, 6210
$m_{\tilde{\nu}_{1,2}}$	3242	4760	3958	7749
$m_{\tilde{\nu}_3}$	3081	4648	3505	7370
$m_{\tilde{e}_{L,R}}$	3256, 3089	4754, 2801	3964, 3367	7742, 6566
$m_{\tilde{\tau}_{1,2}}$	2356, 3089	2360, 4640	2097, 3504	5591, 7355
σ_{SI}(pb)	2.30×10^{-12}	1.85×10^{-11}	3.70×10^{-12}	3.63×10^{-12}
σ_{SD}(pb)	1.11×10^{-10}	3.88×10^{-9}	2.51×10^{-10}	6.93×10^{-10}
$\Omega_{CDM}h^2$	0.114	0.114	0.121	0.055
$R_{tb\tau}$	2.5	3.9	1.73	2.5
$R_{b\tau}$	1.37	1.38	1.44	1.34

Table 2: All the masses are in units of GeV and $\mu < 0$. All points satisfy the sparticle mass bounds, and B-physics constraints described in Section 2. Points 1, 2, 3 and 4 display neutralino-stau, neutralino-stop, A-resonance, and neutralino-gluino coannihilation respectively. Point 4 is the case where relic density is below the WMAP9 5σ bounds.

	Point 1	Point 2	Point 3	Point 4
m_L	4342.3	2443.1	3047.1	2537.4
m_R	3727.6	1830.1	1485.7	2570.6
M_1	-657.78	-886.71	5041.4	-4748.2
M_2	4058.9	-4758.7	1623.6	-2511.2
M_3	2107.5	-2435	5143.7	-5673.4
A_0	-5395.7	3635.3	-2951.9	1813.3
$\tan\beta$	26	18.1	57.2	31.9
$m_{H_u} = m_{H_d}$	5307.9	3954.6	1689.5	1112.0
μ	-333	-312	-5696	-6129
Δ_{EW}	79	38	7807	9039
Δ_{HS}	6869	3813	8100	9082
m_h	126	126	125	125
m_H	5140	4682	1834	5509
m_A	5106	4651	1822	5473
$m_{H^\pm}$	5141	4682	1836	5509
$m_{\tilde{\chi}^0_{1,2}}$	298, 345	307, 323	1347, 2287	2084, 2157
$m_{\tilde{\chi}^0_{3,4}}$	366, 3406	399, 3946	5596, 5596	6157, 6158
$m_{\tilde{\chi}^\pm_{1,2}}$	325, 3367	332, 3920	1350, 5548	2091, 6158
$m_{\tilde{g}}$	4549	5075	10172	11140
$m_{\tilde{u}_{L,R}}$	6208, 5266	5705, 4643	9177, 8827	9826, 9820
$m_{\tilde{t}_{1,2}}$	1924, 4943	2038, 4824	7257, 7896	8226, 8947
$m_{\tilde{d}_{L,R}}$	6208, 5268	5706, 4644	9177, 8767	9827, 9784
$m_{\tilde{b}_{1,2}}$	4775, 5014	4419, 4880	7413, 7856	8907, 9337
$m_{\tilde{\nu}_{1,2}}$	5027	3850	3313	3063
$m_{\tilde{\nu}_3}$	4833	3783	3118	2936
$m_{\tilde{e}_{L,R}}$	5022, 3731	3849, 1849	3322, 2360	3077, 3093
$m_{\tilde{\tau}_{1,2}}$	3161, 4828	1537, 3781	1637, 3112	2793, 2961
σ_{SI}(pb)	9.66×10^{-9}	7.41×10^{-9}	1.02×10^{-12}	2.55×10^{-11}
σ_{SD}(pb)	7.14×10^{-5}	4.72×10^{-5}	1.25×10^{-9}	1.45×10^{-9}
$\Omega_{CDM}h^2$	0.119	0.03	0.091	0.14×10^{-5}
$R_{tb\tau}$	3.55	5.2	1.10	2.0
$R_{b\tau}$	1.37	1.34	1.10	1.37

Table 3: All the masses are in this table are in units of GeV and $\mu < 0$. All this points satisfy the sparticle mass and B-physics constraints described in Section 2. Point 1 represents bino-like neutralino, point 2 displays higgsino like neutralino, point 3 and point 4 are examples of wino-like neutralino. Point 2 and point 4 do not satisfy WMAP9 5σ bounds.

	Point 1	Point 2	Point 3	Point 4
m_L	1992.4	1541.5	3525.1	3632.8
m_R	1598.5	1659.5	3466.1	5259.2
M_1	-507.03	-911.52	-3825.5	6933.9
M_2	-3790.9	-2613.2	-2531.4	1916.5
M_3	-1951.9	-922.33	-2993.5	9495
A_0	2679.3	2189.1	1957.5	525.13
$\tan\beta$	18	22.4	31.7	40.2
$m_{H_u} = m_{H_d}$	3199.1	1676.6	662.98	4072.4
μ	350	1083	4293	8968
Δ_{EW}	32	286	4435	19351
Δ_{HS}	2502	964	4438	22605
m_h	125	123	124	126
m_H	3789	2344	3602	8695
m_A	3765	2328	3578	8638
$m_{H^\pm}$	3790	2345	3603	8696
$m_{\tilde{\chi}^0_{1,2}}$	209, 364	400, 1092	1737, 2124	1537, 3176
$m_{\tilde{\chi}^0_{3,4}}$	366, 3133	1094, 2158	4303, 4304	8853, 8853
$m_{\tilde{\chi}^\pm_{1,2}}$	342, 3101	1067, 2141	2130, 4304	1541, 8767
$m_{\tilde{g}}$	4131	2097	6216	18151
$m_{\tilde{u}_{L,R}}$	4631, 3830	2818, 2406	6451, 6320	15622, 16208
$m_{\tilde{t}_{1,2}}$	1834, 3936	1063, 2321	5001, 5687	13969, 14327
$m_{\tilde{d}_{L,R}}$	4632, 3833	2819, 2402	6451, 6272	15622, 16155
$m_{\tilde{b}_{1,2}}$	3663, 3974	2230, 2340	5646, 5803	14293, 15613
$m_{\tilde{\nu}_{1,2}}$	3104	2269	3915	3952
$m_{\tilde{\nu}_3}$	3053	2215	3794	3566
$m_{\tilde{e}_{L,R}}$	3104, 1603	2268, 1692	3918, 3734	3959, 5821
$m_{\tilde{\tau}_{1,2}}$	1391, 3052	1528, 2212	3467, 3799	3549, 5212
σ_{SI}(pb)	6.00×10^{-10}	1.07×10^{-11}	2.36×10^{-12}	5.58×10^{-14}
σ_{SD}(pb)	1.75×10^{-5}	9.92×10^{-8}	3.35×10^{-10}	1.52×10^{-10}
$\Omega_{CDM}h^2$	1.07	22.3	0.105	0.104
$R_{tb\tau}$	5.31	4.18	2.31	2.86
$R_{b\tau}$	1.33	1.29	1.05	1.91

Table 4: All the masses are in units of GeV and $\mu > 0$. All points satisfy the sparticle mass bounds and B-physics constraints described in Section 2. Points 1-4 respectively correspond to the minimal value of Δ_{EW}, minimal value of Δ_{HS}, best point with b-τ YU, and an example of heavy gluino solution. Points 3 and 4 also satisfy the WMAP9 5σ bounds.

	Point 1	Point 2	Point 3	Point 4
m_L	2517.8	3734.8	2660.3	5549.1
m_R	2187.1	1435	2837.6	7667.2
M_1	1843.3	1871.4	-4493	-3325.8
M_2	1796	1229.6	-3017	-4120.9
M_3	3883	2215.4	-5334.2	-636.94
A_0	-971.61	-5825.6	1714.9	2617.6
$\tan\beta$	56.10	18.90	36.80	51.23
$m_{H_u} = m_{H_d}$	2985.9	4082.3	1226.1	1762.9
μ	3773	2579	5817	4968
Δ_{EW}	3425	1699	8142	5938
Δ_{HS}	5392	5721	8189	6542
m_h	124	127	125	123
m_H	3296	4578	4047	2469
m_A	3248	4548	4021	2453
$m_{H^\pm}$	3271	4578	4048	2470
$m_{\tilde{\chi}^0_{1,2}}$	814, 1488	833, 1033	2046, 2521	1542, 3501
$m_{\tilde{\chi}^0_{3,4}}$	3793, 3793	2587, 2588	5831, 5832	4946, 4948
$m_{\tilde{\chi}^\pm_{1,2}}$	1491, 3793	1032, 2612	2529, 5831	3505, 4939
$m_{\tilde{g}}$	7817	4691	10511	1662
$m_{\tilde{u}_{L,R}}$	7157, 6999	5476, 4206	9413, 9390	6139, 7788
$m_{\tilde{t}_{1,2}}$	5672, 6310	896, 4523	7833, 8321	4343, 6129
$m_{\tilde{d}_{L,R}}$	7158, 6994	5476, 4190	9413, 9349	6140, 7765
$m_{\tilde{b}_{1,2}}$	6264, 6392	3906, 4596	8272, 8479	4417, 6749
$m_{\tilde{\nu}_{1,2}}$	2753	3821	3327	6140
$m_{\tilde{\nu}_3}$	2332	3721	3195	5532
$m_{\tilde{e}_{L,R}}$	2761, 2284	3818, 1569	3334, 3272	6142, 7759
$m_{\tilde{\tau}_{1,2}}$	825, 2333	1009, 3724	2974, 3213	5533, 6765
σ_{SI}(pb)	7.49×10^{-13}	4.31×10^{-12}	1.12×10^{-12}	5.95×10^{-13}
σ_{SD}(pb)	4.21×10^{-10}	1.77×10^{-9}	1.06×10^{-10}	1.68×10^{-10}
$\Omega_{CDM}h^2$	0.137	0.296	0.126	0.178
$R_{tb\tau}$	2.13	4.96	1.83	1.48
$R_{b\tau}$	2.12	1.40	1.08	1.21

Table 5: All the masses are in units of GeV and $\mu > 0$. All points satisfy the sparticle mass bounds, and B-physics constraints described in Section 2. Points 1, 2, 3 and 4 display neutralino-stau, neutralino-stop, A-resonance and neutralino-gluino coannihilation, respectively. Points 2 and 4 are the examples where relic density is little bit above the WMAP9 5σ bounds.

	Point 1	Point 2	Point 3	Point 4
m_L	3620.5	2136.8	2537.4	3216.5
m_R	1475.8	1248.8	2147.6	6057.0
M_1	2080.6	-713.72	5197.6	-5042.8
M_2	1109.9	-3832.9	1992.9	-2293.9
M_3	2398.8	-1991.3	6222.5	-4933.4
A_0	-5687.8	3169.4	-3322.2	-1737.9
$\tan\beta$	16	19	16.57	11.12
$m_{H_u} = m_{H_d}$	4007.4	3358.8	2721.1	3843.9
μ	2812	277	6507	5195
Δ_{EW}	1934	47	10189	6493
Δ_{HS}	5815	2770	11755	9839
m_h	126	126	125	123
m_H	4752	3884	7054	6645
m_A	4720	3859	7008	6602
$m_{H^\pm}$	4752	3885	7055	6646
$m_{\tilde{\chi}^0_{1,2}}$	926, 930	267, 289	1636, 2359	1902,2295
$m_{\tilde{\chi}^0_{3,4}}$	2819, 2820	327, 3178	6430, 6430	5237, 5238
$m_{\tilde{\chi}^\pm_{1,2}}$	927, 2843	272, 3149	1644, 6373	1906, 5233
$m_{\tilde{g}}$	5044	4199	12141	9899
$m_{\tilde{u}_{L,R}}$	5620, 4515	4756, 3755	10601, 10561	8936, 10358
$m_{\tilde{t}_{1,2}}$	1805, 4723	1394, 4003	8684, 9770	7989, 8885
$m_{\tilde{d}_{L,R}}$	5621, 4495	4756, 3756	10602, 10511	8937, 10314
$m_{\tilde{b}_{1,2}}$	4304, 4780	3543, 4055	9728, 10370	8061, 10228
$m_{\tilde{\nu}_{1,2}}$	3697	3218	2925	3610
$m_{\tilde{\nu}_3}$	3626	3159	2864	3573
$m_{\tilde{e}_{L,R}}$	3696, 1642	3217, 1262	2950, 2854	3599, 6325
$m_{\tilde{\tau}_{1,2}}$	1313, 3628	897, 3156	2729, 2886	3580, 6286
σ_{SI}(pb)	2.36×10^{-11}	9.03×10^{-9}	2.03×10^{-12}	8.48×10^{-12}
σ_{SD}(pb)	1.16×10^{-8}	1.32×10^{-4}	6.81×10^{-10}	3.13×10^{-9}
$\Omega_{CDM}h^2$	0.101	0.028	0.109	0.16×10^{-5}
$R_{tb\tau}$	6.05	4.98	6.25	8.2
$R_{b\tau}$	1.41	1.33	1.51	1.25

Table 6: All the masses are in this table are in units of GeV and $\mu > 0$. All this points satisfy the sparticle mass and B-physics constraints described in Section 2. Point 1 represents bino-like neutralino, point 2 displays higgsino like neutralino, point 3 and point 4 are examples of wino-like neutralino. Point 2 and point 4 do not satisfy WMAP9 5σ bounds.